https://doi.org/10.5194/acp-2020-1193
Preprint. Discussion started: 6 January 2021

Atmospheric Chemistry and Physics Discussions

Comprehensive evaluations of diurnal NO_2 measurements during DISCOVER-AQ 2011: Effects of resolution dependent representation of NO_x emissions

Jianfeng Li[1, a], Yuhang Wang[1*], Ruixiong Zhang[1], Charles Smeltzer[1], Andrew Weinheimer[2], Jay Herman[3], K. Folkert Boersma[4, 5], Edward A. Celarier[6, 7, b], Russell W. Long[8], James J. Szykman[8], Ruben Delgado[3], Anne M. Thompson[6], Travis N. Knepp[9, 10], Lok N. Lamsal[6], Scott J. Janz[6], Matthew G. Kowalewski[6], Xiong Liu[11], Caroline R. Nowlan[11]

[1]School of Earth and Atmospheric Sciences, Georgia Institute of Technology, Atlanta, Georgia, USA
[2]National Center for Atmospheric Research, Boulder, Colorado, USA
[3]University of Maryland Baltimore County JCET, Baltimore, Maryland, USA
[4]Royal Netherlands Meteorological Institute, De Bilt, the Netherlands
[5]Wageningen University, Meteorology and Air Quality Group, Wageningen, the Netherlands
[6]NASA Goddard Space Flight Center, Greenbelt, Maryland, USA
[7]Universities Space Research Association, Columbia, Maryland, USA
[8]National Exposure Research Laboratory, Office of Research and Development, U.S. Environmental Protection Agency, Research Triangle Park, NC, USA
[9]NASA Langley Research Center, Virginia, USA
[10]Science Systems and Applications, Inc., Hampton, Virginia, USA
[11]Harvard-Smithsonian Center for Astrophysics, Cambridge, Massachusetts, USA

[a]now at: Atmospheric Sciences and Global Change Division, Pacific Northwest National Laboratory, Richland, Washington, USA
[b]now at: Digital Spec, Tyson's Corner, VA, USA

[*] *Correspondence to* Yuhang Wang (yuhang.wang@eas.gatech.edu)

https://doi.org/10.5194/acp-2020-1193
Preprint. Discussion started: 6 January 2021

Atmospheric Chemistry and Physics Discussions

Abstract

Nitrogen oxides (NO_x = NO + NO_2) play a crucial role in the formation of ozone and secondary inorganic and organic aerosols, thus affecting human health, global radiation budget, and climate. The diurnal and spatial variations of NO_2 are functions of emissions, advection, deposition, vertical mixing, and chemistry. Their observations, therefore, provide useful constraints in our understanding of these factors. We employ a Regional chEmical and trAnsport model (REAM) to analyze the observed temporal (diurnal cycles) and spatial distributions of NO_2 concentrations and tropospheric vertical column densities (TVCDs) using aircraft in situ measurements, surface EPA Air Quality System (AQS) observations, as well as the measurements of TVCDs by satellite instruments (OMI: the Ozone Monitoring Instrument; and GOME-2A: Global Ozone Monitoring Experiment – 2A), ground-based Pandora, and the Airborne Compact Atmospheric Mapper (ACAM) instrument, in July 2011 during the DISCOVER-AQ campaign over the Baltimore-Washington region. The model simulations at 36- and 4-km resolutions are in reasonably good agreement with the temporospatial NO_2 observations in the daytime. However, nighttime mixing in the model needs to be enhanced to reproduce the observed NO_2 diurnal cycle in the model. Another discrepancy is that Pandora measured NO_2 TVCDs show much less variation in the late afternoon than simulated in the model. Relative to the 36-km model simulations, the 4-km model results show larger biases compared to the observations due largely to the larger spatial variations of NO_2 in the model when the spatial resolution is increased from 36 to 4 km, although the biases are often comparable to the ranges of the observations. The high-resolution aircraft ACAM observations show a more dispersed distribution of NO_2 vertical column densities (VCDs) and lower VCDs in urban regions than 4-km model simulations, reflecting likely the spatial distribution bias of NO_x emissions in the National Emissions Inventory (NEI) 2011 at high resolution.

https://doi.org/10.5194/acp-2020-1193
Preprint. Discussion started: 6 January 2021

Atmospheric Chemistry and Physics Discussions

1 Introduction

Nitrogen oxides (NO_x = NO + NO_2) are among the most important trace gases in the atmosphere due to their crucial role in the formation of ozone (O_3), secondary aerosols, and their role in the chemical transformation of other atmospheric species, such as carbon monoxide (CO) and volatile organic compounds (VOCs) (Cheng et al., 2017; Cheng et al., 2018; Fisher et al., 2016; Li et al., 2019; Liu et al., 2012; Ng et al., 2017; Peng et al., 2016; Zhang and Wang, 2016). NO_x is emitted by both anthropogenic activities and natural sources. Anthropogenic sources account for about 77% of the global NO_x emissions, and fossil fuel combustion and industrial processes are the primary anthropogenic sources, which contribute to about 75% of the anthropogenic emissions (Seinfeld and Pandis, 2016). Other important anthropogenic sources include agriculture and biomass and biofuel burning. Soils and lightning are two major natural sources. Most NO_x is emitted as NO, which is then oxidized to NO_2 by oxidants, such as O_3, the hydroperoxyl radical (HO_2), and organic peroxy radicals (RO_2).

The diurnal variations of NO_2 controlled by physical and chemical processes reflect the temporal patterns of these underlying controlling factors, such as NO_x emissions, chemistry, deposition, advection, diffusion, and convection. Therefore, the observations of NO_2 diurnal cycles can be used to evaluate our understanding of NO_x related emission, chemistry, and physical processes (Frey et al., 2013; Jones et al., 2000; Judd et al., 2018). For example, Brown et al. (2004) analyzed the diurnal patterns of surface NO, NO_2, NO_3, N_2O_5, HNO_3, OH, and O_3 concentrations along the East Coast of the United States (U.S.) during the New England Air Quality Study (NEAQS) campaign in the summer of 2002 and found that the predominant nighttime sink of NO_x through the hydrolysis of N_2O_5 had an efficiency on par with daytime photochemical loss over the ocean surface off the New England coast. Van Stratum et al. (2012) investigated the contribution of boundary layer dynamics to chemistry evolution during the DOMINO (Diel Oxidant Mechanisms in relation to Nitrogen Oxides) campaign in 2008 in Spain and found that entrainment and boundary layer growth in daytime influenced mixed-layer NO and NO_2

https://doi.org/10.5194/acp-2020-1193
Preprint. Discussion started: 6 January 2021


Atmospheric Chemistry and Physics Discussions

diurnal cycles on the same order of chemical transformations. David and Nair (2011) found that the diurnal patterns of surface NO, NO_2, and O_3 concentrations at a tropical coastal station in India from November 2007 to May 2009 were closely associated with sea breeze and land breeze which affected the availability of NO_x through transport. They also thought that monsoon-associated synoptic wind patterns could strongly influence the magnitudes of NO, NO_2, and O_3 diurnal cycles. The monsoon effect on surface NO, NO_2, and O_3 diurnal cycles was also observed in China by Tu et al. (2007) on the basis of continuous measurements of NO, NO_2, and O_3 at an urban site in Nanjing from January 2000 – February 2003.

In addition to surface NO_2 diurnal cycles, the daily variations of NO_2 vertical column densities (VCDs) were also investigated in previous studies. For example, Boersma et al. (2008) compared NO_2 tropospheric VCDs (TVCDs) retrieved from OMI (the Ozone Monitoring Instrument) and SCIAMACHY (SCanning Imaging Absorption SpectroMeter for Atmospheric CHartography) in August 2006 around the world. They found that the diurnal patterns of different types of NO_x emissions could strongly affect the NO_2 TVCD variations between OMI and SCIAMACHY and that intense afternoon fire activity resulted in an increase of NO_2 TVCDs from 10:00 LT (local time) to 13:30 LT over tropical biomass burning regions. Boersma et al. (2009) further investigated the NO_2 TVCD change from SCIAMACHY to OMI in different seasons of 2006 in Israeli cities and found that there was a slight increase of NO_2 TVCDs from SCIAMACHY to OMI in winter due to increased NO_x emissions from 10:00 LT to 13:30 LT and a sufficiently weak photochemical sink and that the TVCDs from OMI were lower than SCIAMACHY in summer due to a strong photochemical sink of NO_x.

All these above researches, however, exploited only NO_2 surface or satellite VCD measurements. Knepp et al. (2015) related the daytime variations of NO_2 TVCD measurements by ground-based Pandora instruments to the variations of coincident NO_2 surface concentrations using a planetary boundary layer height (PBLH) factor over the periods July 2011 – October 2011 at the NASA Langley Research Center in Hampton, Virginia and July

https://doi.org/10.5194/acp-2020-1193
Preprint. Discussion started: 6 January 2021


Atmospheric Chemistry and Physics Discussions

2011 at Padonia and Edgewood sites in Maryland for the DISCOVER-AQ experiment, showing the importance of boundary-layer vertical mixing on NO_2 vertical distributions and the ability of NO_2 VCD measurements to infer hourly boundary-layer NO_2 variations. DISCOVER-AQ, the Deriving Information on Surface conditions from Column and Vertically Resolved Observations Relevant to Air Quality experiment (https://discover-aq.larc.nasa.gov/), was designed to better understand the relationship between boundary-layer pollutants and satellite observations (Flynn et al., 2014; Reed et al., 2015). Figure S1 shows the sampling locations of the summer DISCOVER-AQ 2011 campaign in the Baltimore-Washington metropolitan region. In this campaign, the NASA P-3B aircraft flew spirals over six air quality monitoring sites (Aldino - rural/suburban, Edgewood - coastal/urban, Beltsville - suburban, Essex - coastal/urban, Fairhill - rural, and Padonia - suburban) (Table S1) and the Chesapeake Bay (Cheng et al., 2017; Lamsal et al., 2014), and measured 244 NO_2 profiles in 14 flight days in July (Zhang et al., 2016). During the same period, the NASA UC-12 aircraft flew across the Baltimore-Washington region at an altitude about 8 km above sea level (ASL), using the Airborne Compact Atmospheric Mapper (ACAM) to map the distributions of NO_2 VCDs below the aircraft (Lamsal et al., 2017). Furthermore, ground-based instruments were deployed to measure NO_2 surface concentrations, NO_2 VCDs, and other physical properties of the atmosphere (Anderson et al., 2014; Reed et al., 2015; Sawamura et al., 2014). Satellite OMI and GOME-2A (Global Ozone Monitoring Experiment – 2A) instruments provided NO_2 TVCD measurements over the campaign region at 13:30 and 9:30 LT, respectively. These concurrent measurements of NO_2 VCDs, surface NO_2, and vertically resolved distributions of NO_2 during the DISCOVER-AQ 2011 campaign, therefore, provide a comprehensive dataset to evaluate NO_2 diurnal and spatial variabilities and processes affecting NO_2 concentrations.

Section 2 describes the measurement datasets in detail. The Regional chEmistry and trAnsport Model (REAM), also described in section 2, is applied to simulate the NO_2 observations during the DISCOVER-AQ campaign in July 2011. The evaluations of the simulated diurnal cycles of surface NO_2 concentrations, NO_2

https://doi.org/10.5194/acp-2020-1193
Preprint. Discussion started: 6 January 2021


Atmospheric Chemistry and Physics Discussions

vertical profiles, and NO_2 TVCDs are discussed in section 3 through comparisons with observations. In section 3, we also investigate the differences between NO_2 diurnal cycles on weekdays and weekends and their implications for NO_x emission characteristics. To corroborate our evaluation of NO_x emissions based on NO_2 diurnal cycles, we further compare observed NO_y (reactive nitrogen compounds) concentrations with REAM simulation results in section 3. Moreover, we assess the resolution dependence of REAM simulation results in light of the observations and discuss the potential biases of NO_x emissions at high resolution by comparing the 4-km REAM simulation results with high-resolution ACAM NO_2 VCDs. Finally, we summarize the study in section 4.

2 Datasets and model description

2.1 REAM

REAM has been widely applied in many studies (Cheng et al., 2017; Choi et al., 2008; Li et al., 2019; Zhang et al., 2018; Zhang et al., 2016; Zhao et al., 2009). The model has a horizontal resolution of 36 km and 30 vertical layers in the troposphere. Meteorology fields are from a Weather Research and Forecasting (WRF, version 3.6) model simulation with a horizontal resolution of 36 km. We summarize the physics parameterization schemes of the WRF simulation in Table S2. The WRF simulation is initialized and constrained by the NCEP coupled forecast system model version 2 (CFSv2) products (http://rda.ucar.edu/datasets/ds094.0/) (Saha et al., 2011). The chemistry mechanism in REAM is based on GEOS-Chem v11.01 with updated aerosol uptake of isoprene nitrates (Fisher et al., 2016) and revised treatment of wet scavenging processes (Luo et al., 2019). A 2° × 2.5° GEOS-Chem simulation provides the chemical boundary and initial conditions.

Biogenic VOC emissions in REAM are from MEGAN v2.10 (Guenther et al., 2012). Anthropogenic emissions on weekdays are from the National Emission Inventory 2011 (NEI2011) (EPA, 2014) from the Pacific Northwest National Laboratory (PNNL), which has an initial resolution of 4 km and is re-gridded to REAM 36-

https://doi.org/10.5194/acp-2020-1193
Preprint. Discussion started: 6 January 2021


Atmospheric Chemistry and Physics Discussions

km grid cells (Figure S2). Weekday emission diurnal profiles are from NEI2011. The weekday to weekend emission ratios and weekend emission diurnal profiles are based on previous studies (Beirle et al., 2003; Boersma et al., 2009; Choi et al., 2012; de Foy, 2018; DenBleyker et al., 2012; Herman et al., 2009; Judd et al., 2018; Kaynak et al., 2009; Kim et al., 2016). These studies suggested that weekend NO_x emissions were 20% - 50% lower than weekday emissions, and the weekend NO_x emission diurnal cycles were different from weekdays; therefore, we specify a weekend to weekday NO_x emission ratio of 2/3 in this study. The resulting diurnal variations of weekday and weekend NO_x emissions over the DISCOVER-AQ 2011 region are shown in Figure 1. The diurnal emission variation is lower on weekends than on weekdays.

To understand the effects of model resolutions on the temporospatial distributions of NO_2, we also conduct a REAM simulation with a horizontal resolution of 4 km during the DISCOVER-AQ campaign. A 36-km REAM simulation (discussed in section 3.1) provides the chemical initial and hourly boundary conditions. Meteorology fields are from a nested WRF simulation (36 km, 12 km, 4 km) with cumulus parameterization turned off in the 4-km domain (Table S2). Figure S1 shows a comparison of the 4-km and 36-km REAM grid cells with DISCOVER-AQ observations, and Figure S2 shows a comparison of NO_x emission distributions between the 4-km and 36-km REAM simulations. The comparison of NO_x emission diurnal variations over the DISCOVER-AQ 2011 region between the 4-km and 36-km REAM is shown in Figure 1.

We evaluate the performances of the 36-km and nested 4-km WRF simulations by comparing temperature and wind from the P-3B spirals (Figure S1) and precipitation from the NCEP (National Centers for Environmental Prediction) Stage IV precipitation dataset with those coincident WRF simulation results in July 2011. Generally, P-3B spirals range from ~400 m to ~3.63 km in height above the ground level (AGL). As shown in Figure S3, both the 36-km and nested 4-km WRF simulations predict temperature well with $R^2 = 0.94$ and $R^2 = 0.98$, respectively. Both WRF simulations show good agreement with P-3B measurements in U-wind (36-km: R^2

https://doi.org/10.5194/acp-2020-1193
Preprint. Discussion started: 6 January 2021


Atmospheric Chemistry and Physics Discussions

157 = 0.62; 4-km: R^2 = 0.71), V-wind (36-km: R^2 = 0.75; 4-km: R^2 = 0.74), wind speed (36-km: R^2 = 0.52; 4-km: R^2
158 = 0.64), and wind direction (36-km: R^2 = 0.40; 4-km: R^2 = 0.50) (Figures S3 and S4). The evaluations above
159 suggest that WRF simulated wind fields are good and comparable at 4-km and 36-km resolutions; they are not the
160 reasons for the differences of the 4-km and 36-km simulations of trace gases by REAM, which is driven by WRF
161 meteorological fields.

162 The NCEP Stage IV precipitation dataset provides hourly precipitation across the contiguous United States
163 (CONUS) with a resolution of ~4 km based on the merging of rain gauge data and radar observations (Lin and
164 Mitchell, 2005; Nelson et al., 2016). The Stage IV dataset is useful for evaluating model simulations, satellite
165 precipitation estimates, and radar precipitation estimates (Davis et al., 2006; Gourley et al., 2011; Kalinga and
166 Gan, 2010; Lopez, 2011; Yuan et al., 2008). We obtain the Stage IV precipitation data in July 2011 from the
167 NCAR/UCAR Research Data Archive (https://rda.ucar.edu/datasets/ds507.5/). As shown in Figures S5 and S6,
168 generally, both the 36-km and nested 4-km WRF simulations predict much less precipitation (in precipitation
169 amount and duration) compared to Stage-IV in July 2011 around the DISCOVER-AQ campaign region,
170 especially for the nested 4-km WRF simulation. We find that large-scale precipitation amounts are much less
171 compared to convective precipitation in most regions in the 36-km WRF simulation (Figure S7) during the
172 simulation period, which is contradictory to Li et al. (2020) showing non-convective precipitation accounting for
173 25% − 40% of the total precipitation. At 4-km resolution, convective and non-convective precipitations are not
174 separated because convection is explicitly resolved. The model low bias is large (Figure S6). The underestimation
175 of precipitation in our WRF simulations may lead to high biases of soluble species in REAM, such as HNO_3, due
176 to underestimated wet scavenging.

https://doi.org/10.5194/acp-2020-1193
Preprint. Discussion started: 6 January 2021


Atmospheric Chemistry and Physics Discussions

2.2 NO_2 TVCD measurements by OMI and GOME-2A

The OMI instrument onboard the sun-synchronous NASA EOS Aura satellite with an equator-crossing time of around 13:30 LT was developed by the Finnish Meteorological Institute and the Netherlands Agency for Aerospace Programs to measure solar backscattering radiation in the visible and ultraviolet bands (Levelt et al., 2006; Russell et al., 2012). The radiance measurements are used to derive trace gas concentrations in the atmosphere, such as O_3, NO_2, HCHO, and SO_2 (Levelt et al., 2006). OMI has a nadir resolution of 13 km × 24 km and provides daily global coverage (Levelt et al., 2006).

Two widely-used archives of OMI NO_2 VCD products are available, NASA OMNO2 (v4.0) (https://disc.gsfc.nasa.gov/datasets/OMNO2_003/summary) and KNMI DOMINO (v2.0) (http://www.temis.nl/airpollution/no2.html). Although both use Differential Optical Absorption Spectroscopy (DOAS) algorithms to derive NO_2 slant column densities, they have differences in spectral fitting, stratospheric and tropospheric NO_2 slant column density (SCD) separation, a priori NO_2 vertical profiles, and air mass factor (AMF) calculation, etc. (Boersma et al., 2011; Bucsela et al., 2013; Chance, 2002; Krotkov et al., 2017; Lamsal et al., 2020; Marchenko et al., 2015; Oetjen et al., 2013; van der A et al., 2010; Van Geffen et al., 2015). Both OMNO2 and DOMINO have been extensively evaluated with field measurements and models (Boersma et al., 2009; Boersma et al., 2011; Choi et al., 2020; Hains et al., 2010; Huijnen et al., 2010; Ionov et al., 2008; Irie et al., 2008; Lamsal et al., 2014; Lamsal et al., 2020; Oetjen et al., 2013). The estimated uncertainty of DOMINO TVCD product is 1.0×10^{15} molecules cm^{-2} + 25% (Boersma et al., 2011), while the uncertainty of OMNO2 TVCD product ranges from ~30% under clear-sky conditions to ~60% under cloudy conditions (Lamsal et al., 2014; Oetjen et al., 2013; Tong et al., 2015). In order to reduce uncertainties in this study, we only use TVCD data with effective cloud fractions < 0.2. The data affected by row anomaly are excluded (Boersma et al., 2018; Zhang et al., 2018).

https://doi.org/10.5194/acp-2020-1193
Preprint. Discussion started: 6 January 2021


Atmospheric Chemistry and Physics Discussions

For AMF calculation, DOMINO used daily TM4 model results with a resolution of 3° × 2° as a priori NO_2 vertical profiles (Boersma et al., 2007; Boersma et al., 2011), while OMNO2 v4.0 used monthly mean values from the Global Modeling Initiative (GMI) model with a resolution of 1° × 1.25°. The relatively coarse horizontal resolution of the a priori NO_2 profiles in the retrievals can introduce uncertainties in the spatial and temporal characteristics of NO_2 TVCDs at satellite pixel scales. For comparison purposes, we also use 36-km REAM simulation results as the a priori NO_2 profiles to compute the AMFs and NO_2 TVCDs with the DOMINO algorithm.

The GOME-2 instrument onboard the polar-orbiting MetOp-A satellite (now referred to as GOME-2A) is an improved version of GOME-1 launched in 1995 and has an overpass time of 9:30 LT and a spatial resolution of 80 × 40 km^2 (Munro et al., 2006; Peters et al., 2012). GOME-2A measures backscattered solar radiation in the range from 240 nm to 790 nm, which is used for VCD retrievals of trace gases, such as O_3, NO_2, BrO, and SO_2 (Munro et al., 2006). We use the KNMI TM4NO2A v2.3 GOME-2A NO_2 VCD product archived on http://www.temis.nl/airpollution/no2col/no2colgome2_v2.php (Boersma et al., 2007; Boersma et al., 2011). GOME-2A derived NO_2 VCDs have been validated with SCIAMACHY and MAX-DOAS measurements (Irie et al., 2012; Peters et al., 2012; Richter et al., 2011). As in the case of OMI, we also recalculate the AMF values and GOME-2A TVCDs using the daily 36-km REAM NO_2 profiles (9:00 LT – 10:00 LT).

2.3 Pandora ground-based NO_2 VCD measurements

Pandora is a small direct sun spectrometer, which measures sun and sky radiance from 270 to 530 nm with a 0.5 nm resolution and a 1.6° field of view (FOV) for the retrieval of the total VCDs of NO_2 with a precision of about 2.7 × 10^{14} molecules/cm^2 and a nominal accuracy of 2.7 × 10^{15} molecules cm^{-2} under clear-sky conditions (Herman et al., 2009; Lamsal et al., 2014). There were 12 Pandora sites operating in the DISCOVER-AQ campaign (Figure S1). Six of them are the same as the P-3B aircraft spiral locations (Aldino, Edgewood,

https://doi.org/10.5194/acp-2020-1193
Preprint. Discussion started: 6 January 2021


Atmospheric Chemistry and Physics Discussions

Beltsville, Essex, Fairhill, and Padonia) (Table S1 and Figure S1). The other six sites are Naval Academy (Annapolis Maryland) (USNA – ocean), University of Maryland College Park (UMCP – urban), University of Maryland Baltimore County (UMBC – urban), Smithsonian Environmental Research Center (SERC – rural/coastal), Oldtown in Baltimore (Oldtown – urban), and Goddard Space Flight Center (GSFC – urban/suburban) (Table S1 and Figure S1). In this study, we exclude the USNA site as its measurements were conducted on a ship ("Pandora(w)" in Figure S1), and there were no other surface observations in the corresponding REAM grid cell. Including the data from the USNA site has a negligible effect on the comparisons of observed and simulated NO_2 TVCDs. In our analysis, we ignore Pandora measurements with solar zenith angles (SZA) > 80° (Figure S8) and exclude the data when fewer than three valid measurements are available within an hour to reduce the uncertainties of the hourly averages due to the significant variations of Pandora observations (Figure S9).

Since Pandora measures total NO_2 VCDs, we need to subtract stratosphere NO_2 VCDs from the total VCDs to compute TVCDs. As shown in Figure S10, stratosphere NO_2 VCDs show a clear diurnal cycle with an increase during daytime due in part to the photolysis of reactive nitrogen reservoirs such as N_2O_5 and HNO_3 (Brohede et al., 2007; Dirksen et al., 2011; Peters et al., 2012; Sen et al., 1998; Spinei et al., 2014), which is consistent with the significant increase of stratospheric NO_2 VCDs from GOME-2A to OMI. In this study, we use the GMI model simulated stratospheric NO_2 VCDs in Figure S10 to calculate the Pandora NO_2 TVCDs. The small discrepancies between the GMI stratospheric NO_2 VCDs and satellite products do not change the pattern of Pandora NO_2 TVCD diurnal variations or affect the conclusions in this study.

2.4 ACAM NO_2 VCD measurements

The ACAM instrument onboard the UC-12 aircraft consists of two thermally spectrometers in the ultraviolet/visible/near-infrared range. The spectrometer in the ultraviolet/visible band (304 nm – 520 nm) with a

https://doi.org/10.5194/acp-2020-1193
Preprint. Discussion started: 6 January 2021


Atmospheric Chemistry and Physics Discussions

resolution of 0.8 nm and a sampling of 0.105 nm can be used to detect NO_2 in the atmosphere. The native ground resolution of UC-12 ACAM NO_2 measurements is 0.5 km × 0.75 km at a flight altitude of about 8 km ASL and a nominal ground speed of 100 m s^{-1} during the DISCOVER-AQ 2011 campaign (Lamsal et al., 2017), thus providing high-resolution NO_2 VCDs below the aircraft.

In this study, we mainly use the ACAM NO_2 VCD product described by Lamsal et al. (2017), which applied a pair-average co-adding scheme to produce NO_2 VCDs at a ground resolution of about 1.5 km (cross-track) × 1.1 km (along-track) to reduce noise impacts. In their retrieval of ACAM NO_2 VCDs, they first used the DOAS fitting method to generate differential NO_2 SCDs relative to the SCDs at an unpolluted reference location. Then they computed above/below-aircraft AMFs at both sampling and reference locations based on the vector linearized discrete ordinate radiative transfer code (VLIDORT) (Spurr, 2008). In the computation of AMFs, the a priori NO_2 vertical profiles were from a combination of a high-resolution (4-km) CMAQ (the Community Multiscale Air Quality Modeling System) model outputs in the boundary layer and a GMI simulation (2° × 2.5°) results elsewhere in the atmosphere. Finally, the below-aircraft NO_2 VCDs at the sampling locations were generated by dividing below-aircraft NO_2 SCDs at the sampling locations by the corresponding below-aircraft AMFs. The below-aircraft NO_2 SCDs were the differences between the total and above-aircraft NO_2 SCDs. The total NO_2 SCDs were the sum of DOAS fitting generated differential NO_2 SCDs and NO_2 SCDs at the reference location, and the above-aircraft NO_2 SCDs were derived based on above-aircraft AMFs, GMI NO_2 profiles, and OMNO2 stratospheric NO_2 VCDs (Lamsal et al., 2017). The ACAM NO_2 VCD product had been evaluated via comparisons with other independent observations during the DISCOVER-AQ 2011 campaign, such as P-3B aircraft, Pandora, and OMNO2, and the uncertainty of individual below-aircraft NO_2 VCD is about 30% (Lamsal et al., 2017). To keep the consistency of ACAM NO_2 VCDs, we exclude NO_2 VCDs measured at altitudes < 8 km ASL, which accounts for about 6.8% of the total available ACAM NO_2 VCD data. We regrid the 1.5 km × 1.1 km ACAM NO_2 VCDs to the 4-km REAM grid cells (Figure S1), which are then used to evaluate the distribution

https://doi.org/10.5194/acp-2020-1193
Preprint. Discussion started: 6 January 2021


Atmospheric Chemistry and Physics Discussions

of NO_2 VCDs in the 4-km REAM simulation. As a supplement in section 3.6, we also assess the 4-km REAM simulation by using the UC-12 ACAM NO_2 VCDs produced by the Smithsonian Astrophysical Observatory (SAO) algorithms, archived on https://www-air.larc.nasa.gov/cgi-bin/ArcView/discover-aq.dc-2011?UC12=1#LIU.XIONG/ (Liu et al., 2015a; Liu et al., 2015b). This product is an early version of the SAO algorithm used to produce the Geostationary Trace gas and Aerosol Sensor Optimization (GeoTASO) and the GEOstationary Coastal and Air Pollution Events (GEO-CAPE) Airborne Simulator (GCAS) airborne observations in later airborne campaigns (Nowlan et al., 2016; Nowlan et al., 2018).

2.5 Surface NO_2 and O_3 measurements

The measurement of NO_x is based on the chemiluminescence of electronically excited NO_2^*, produced from the reaction of NO with O_3, and the strength of the chemiluminescence from the decay of NO_2^* to NO_2 is proportional to the number of NO molecules present (Reed et al., 2016). NO_2 concentrations can be measured with this method by converting NO_2 to NO first through catalytic reactions (typically on the surface of heated molybdenum oxide (MoO_x) substrate) or photolytic processes (Lamsal et al., 2015; Reed et al., 2016). However, for the catalytic method, reactive nitrogen compounds other than NO_x (NO_z), such as HNO_3, peroxyacetyl nitrate (PAN), and other organic nitrates, can also be reduced to NO on the heated surface, thus causing an overestimation of NO_2. The magnitude of the overestimation depends on the concentrations and the reduction efficiencies of interference species, both of which are uncertain. The photolytic approach, which employs broadband photolysis of ambient NO_2, offers more accurate NO_2 measurements (Lamsal et al., 2015).

There were 11 NO_x monitoring sites operating in the DISCOVER-AQ region during the campaign (Figure S1), including those from the EPA Air Quality System (AQS) monitoring network and those deployed for the DISCOVER-AQ campaign. Nine of them measured NO_2 concentrations by a catalytic converter. The other two sites (Edgewood and Padonia) had NO_2 measurements from both catalytic and photolytic methods. Different

https://doi.org/10.5194/acp-2020-1193
Preprint. Discussion started: 6 January 2021


Atmospheric Chemistry and Physics Discussions

288 stationary catalytic instruments were used during the campaign: Thermo Electron 42C-Y NO_y analyzer, Thermo
289 Model 42C NO_x analyzer, Thermo Model 42I-Y NO_y analyzer, and Ecotech Model 9843/9841 T-NO_y analyzers.
290 In addition, a mobile platform — NATIVE (Nittany Atmospheric Trailer and Integrated Validation Experiment)
291 with a Thermo Electron 42C-Y NO_y analyzer installed, was also deployed in the Edgewood site. The photolytic
292 measurements of NO_2 in Edgewood and Padonia were from Teledyne API model 200eup photolytic NO_x
293 analyzers. We scale catalytic NO_2 measurements using the diurnal ratios of NO_2 photolytic measurements to NO_2
294 from the corresponding catalytic analyzers (Figure 2). Figure 2 shows the lowest photolytic/catalytic ratios in the
295 afternoon, which reflects the production of nitrates and other reactive nitrogen compounds from NO_x in the
296 daytime. When photolytic measurements are available, we only use the photolytic observations in this study;
297 otherwise, we use the scaled catalytic measurements.

298 Nineteen surface O_3 monitoring sites were operating in the DISCOVER-AQ region during the campaign
299 (Figure S1). They measured O_3 concentrations by using a Federal Equivalent Method (FEM) based on the UV
300 absorption of O_3 (https://www.arb.ca.gov/aaqm/qa/qa-manual/vol4/chapter6o3.pdf) with an uncertainty of 5 ppb.

301 2.6 Aircraft measurements of NO_2 vertical profiles

302 In this study, we mainly use the NO_2 concentrations measured by the National Center for Atmospheric
303 Research (NCAR) 4-channel chemiluminescence instrument (P-CL) onboard the P-3B aircraft for the evaluation
304 of REAM simulated NO_2 vertical profiles. The instrument has a NO_2 measurement uncertainty of 10% – 15% and
305 a 1-second, 1-sigma detection limit of 30 pptv.

306 NO_2 measurements from aircraft spirals provide us with NO_2 vertical profiles. Figure S1 shows the locations
307 of the aircraft spirals during the DISCOVER-AQ campaign, except for the Chesapeake Bay spirals over the
308 ocean. There were only six spirals available over the Chesapeake Bay, which have ignorable impacts on the

https://doi.org/10.5194/acp-2020-1193
Preprint. Discussion started: 6 January 2021


Atmospheric Chemistry and Physics Discussions

following analyses. Therefore, we do not use them in this study. The rest 238 spirals in the daytime for July 2011 are used to compute the average profiles of NO_2 for the six inland sites (Figure S1).

The aircraft measurements were generally sampled from about a height of 400 m AGL in the boundary layer to 3.63 km AGL in the free troposphere. We bin these measurements to REAM vertical levels. In order to make up the missing observations between the surface and 400 m, we apply quadratic polynomial regressions by using aircraft data below 1 km and coincident NO_2 surface measurements.

In addition to using NO_2 concentrations from the NCAR 4-channel instrument to evaluate REAM simulated NO_2 vertical profiles, we also use P-3B NO, NO_2, and NO_y concentrations measured by the NCAR 4-channel instrument and NO_2, total peroxyacyl nitrates ($\sum$PNs), total alkyl nitrates ($\sum$ANs) (include alkyl nitrates and hydroxyalkyl nitrates), and HNO_3 concentrations measured by the thermal dissociation-laser induced fluorescence (TD-LIF) technique (Day et al., 2002; Thornton et al., 2000; Wooldridge et al., 2010) to evaluate the concentrations of NO_y from REAM (Table 1). All these P-3B measurements are vertically binned to REAM grid cells for comparisons with REAM results. In addition, below the P-3B spirals, four NO_y observation sites at Padonia, Edgewood, Beltsville, and Aldino were operating to provide continuous hourly NO_y surface concentrations during the campaign, which we also use to evaluate REAM simulated NO_y surface concentrations in this study. We summarize the information of available observations at the 11 inland Pandora sites in Table S1.

https://doi.org/10.5194/acp-2020-1193
Preprint. Discussion started: 6 January 2021

Atmospheric Chemistry and Physics Discussions

3 Results and discussion

3.1 Effect of boundary layer vertical mixing on the diurnal variations of surface NO_2 concentrations

3.1.1 36-km model simulation in comparison to the surface observations

Figures 3a and 3b show the observed and 36-km REAM simulated diurnal cycles of surface NO_2 and O_3 concentrations on weekdays in July 2011 in the DISCOVER-AQ region. REAM with WRF simulated vertical diffusion coefficient (k_{zz}) values significantly overestimates NO_2 concentrations and underestimates O_3 concentrations at night, although it captures the patterns of the diurnal cycles of surface NO_2 and O_3: an O_3 peak and a NO_2 minimum around noontime. At night, the reaction of $O_3 + NO \rightarrow O_2 + NO_2$ produces NO_2 but removes O_3. Since most NO_x emissions are in the form of NO, the model biases of low O_3 and high NO_2 occur at the same time. Since there are no significant chemical sources of O_3 at night, mixing of O_3 rich air above the surface is the main source of O_3 supply near the surface. Therefore, the nighttime model biases with WRF simulated k_{zz} data in Figure 3 indicate that vertical mixing may be underestimated at night.

During the DISCOVER-AQ campaign, WRF simulated vertical wind velocities are very low at night and have little impact on vertical mixing (Figure S11a). The nighttime vertical mixing is mainly attributed to turbulent mixing. In the Yonsei University (YSU) planetary boundary layer (PBL) scheme (Shin and Hong, 2011) used by our WRF simulations (Table S2), boundary layer k_{zz} is correlated to PBLH. However, Breuer et al. (2014) and Hu et al. (2012) found that the YSU scheme underestimated nighttime PBLHs in WRF, which is consistent with Figure 4 showing that YSU k_{zz}-determined PBLHs are significantly lower than lidar observations in the late afternoon and at night at the UMBC site during the DISCOVER-AQ campaign. The lidar mixing depth data were derived from the Elastic Lidar Facility (ELF) attenuated backscatter signals by using the covariance wavelet transform method and had been validated against radiosonde measurements, Radar wind profiler

https://doi.org/10.5194/acp-2020-1193
Preprint. Discussion started: 6 January 2021


Atmospheric Chemistry and Physics Discussions

346 observations, and Sigma Space mini-micropulse lidar data (Compton et al., 2013). To improve nighttime PBLHs
347 and vertical mixing in REAM, we increase REAM k_{zz} below 500 m during 18:00 – 5:00 LT to 5 m s^{-2} if the WRF
348 computed k_{zz} < 5 m s^{-2}, which significantly increases the PBLHs at night (Figure 4), leading to the decreases of
349 simulated surface NO_2 and the increases of surface O_3 concentrations at night (Figure 3). The assigned value of 5
350 m s^{-2} is arbitrary. Changing this value to 2 or 10 m s^{-2} can also alleviate the biases of model simulated nighttime
351 surface NO_2 and O_3 concentrations. An alternative solution to correct the model nighttime simulation biases is to
352 reduce NO_x emissions by 50-67%, but we cannot find good reasons to justify this level of NO_x emission
353 reduction only at night.

354 The updated REAM simulation of surface NO_2 diurnal pattern in Figure 3a is in good agreement with
355 previous studies (Anderson et al., 2014; David and Nair, 2011; Gaur et al., 2014; Reddy et al., 2012). Daytime
356 surface NO_2 concentrations are much lower compared to nighttime, and NO_2 concentrations reach a minimum
357 around noontime. As shown in Figure S12, under the influence of vertical turbulent mixing, the surface-layer
358 NO_x emission diurnal pattern is similar to the surface NO_2 diurnal cycle in Figure 3a, emphasizing the importance
359 of turbulent mixing on modulating surface NO_2 diurnal variations. The highest boundary layer (Figure 4) due to
360 solar radiation leads to the lowest surface-layer NO_x emissions (Figure S12) and, therefore, the smallest surface
361 NO_2 concentrations occur around noontime (Figure 3a). Transport, which is mainly attributed to advection and
362 turbulent mixing, is another critical factor affecting surface NO_2 diurnal variations (Figure S12). The magnitudes
363 of transport fluxes (Figure S12) are proportional to horizontal and vertical gradients of NO_x concentrations and
364 are therefore generally positively correlated to surface NO_2 concentrations. However, some exceptions exist,
365 reflecting different strengths of advection (U, V, and W) and turbulent mixing (k_{zz}) at different times. For
366 example, in the early morning, NO_2 surface concentrations peak at 5:00 – 6:00 LT (Figure 3a), while transport
367 fluxes peak at 7:00 – 8:00 LT (Figure S12). The delay of the peak is mainly due to lower turbulent mixing at 5:00
368 – 6:00 LT than other daytime hours in the model (Figure 4). Chemistry also contributes to surface NO_2 diurnal

https://doi.org/10.5194/acp-2020-1193
Preprint. Discussion started: 6 January 2021


Atmospheric Chemistry and Physics Discussions

variations mainly through photochemical sinks in the daytime and N_2O_5 hydrolysis at nighttime. Chemistry fluxes in Figure S12 are not only correlated to the strength of photochemical reactions and N_2O_5 hydrolysis (chemistry fluxes per unit NO_x) but are also proportional to NO_x surface concentrations. Therefore, chemistry fluxes in Figure S12 cannot directly reflect the impact of solar radiation on photochemical reactions. It can, however, still be identified by comparing afternoon chemistry contributions: from 13:00 to 15:00 LT, surface-layer NO_x emissions and NO_2 concentrations are increasing (Figures S12 and 3a); however, chemistry losses are decreasing as a result of the reduction of photochemical sinks with weakening solar radiation. The contributions of vertical mixing and photochemical sinks to NO_2 concentrations can be further corroborated by daytime variations of NO_2 vertical profiles (Figure 6) and TVCDs (Figure S13) discussed in sections 3.2 and 3.3.

Figure 3c shows the diurnal variation on weekends is also simulated well in the improved 36-km model. The diurnal variation of surface NO_2 concentrations (REAM: 1.5 – 10.4 ppb; observations: 2.1 – 9.8 ppb) is lower than on weekdays (REAM: 2.5 – 12.5 ppb; observations: 3.3 – 14.5 ppb), reflecting lower magnitude and variation of NO_x emissions on weekends (Figure 1). Figure 3d also shows an improved simulation of surface O_3 concentrations at nighttime due to the improved PBLH simulation (Figure 4).

3.1.2 4-km model simulation in comparison to the surface observations

The results of 4-km REAM simulations with original WRF k_{zz} (not shown) are very similar to Figure 3 since WRF simulated nocturnal vertical mixing is insensitive to the model horizontal resolution. Applying the modified nocturnal mixing in the previous section also greatly reduced the nighttime NO_2 overestimate and O_3 underestimate in the 4-km REAM simulations. All the following analyses are based on REAM simulations with improved nocturnal mixing. Figure 5 shows that mean surface NO_2 concentrations simulated in the 4-km model are higher than the 36-km results over Padonia, Oldtown, Essex, Edgewood, Beltsville, and Aldino (Table S1),

https://doi.org/10.5194/acp-2020-1193
Preprint. Discussion started: 6 January 2021


Atmospheric Chemistry and Physics Discussions

390 leading to higher biases compared to the observations at night. A major cause is that the observation sites are
391 located in regions of high NO_x emissions (Figures S1 and S2). At a higher resolution of 4 km, the high emissions
392 around the surface sites are apparent compared to rural regions. At the coarser 36-km resolution, spatial
393 averaging greatly reduces the emissions around the surface sites. On average, NO_x emissions (molecules km^{-2} s^{-1})
394 around the six surface NO_2 observations sites are 67% higher in the 4-km than the 36-km REAM simulations
395 (Table S1). The resolution dependence of model results will be further discussed in the model evaluations using
396 the other in situ and remote sensing measurements.

397 3.2 Diurnal variations of NO_2 vertical profiles

398 Figures 6a and 6c show the temporal variations of P-3B observed and 36-km REAM simulated NO_2 vertical
399 profiles in the daytime on weekdays during the DISCOVER-AQ campaign. 36-km REAM reproduces well the
400 observed characteristics of NO_2 vertical profiles in the daytime (R^2 = 0.91), which are strongly affected by
401 vertical mixing and photochemistry (Zhang et al., 2016). When vertical mixing is weak in the early morning
402 (6:00 – 8:00 LT), NO_2, released mainly from surface NO_x sources, is concentrated in the surface layer, and the
403 vertical gradient is large. As vertical mixing becomes stronger after 8:00 LT, NO_2 concentrations below 500 m
404 decrease significantly, while those over 500 m increase from 6:00 – 8:00 LT to 12:00 – 14:00 LT. It is
405 noteworthy that PBLHs and NO_x emissions are comparable between 12:00 – 14:00 LT and 15:00 – 17:00 LT
406 (Figures 1 and 4); however, NO_2 concentrations at 15:00 – 17:00 LT are significantly higher than at 12:00 –
407 14:00 LT in the whole boundary layer, reflecting the impact of the decreased photochemical loss of NO_x in the
408 late afternoon. In fact, photochemical losses affect all the daytime NO_2 vertical profiles, which can be easily
409 identified by NO_2 TVCD process diagnostics discussed in section 3.3 (Figure S13).

410 Figures 6b and 6d also show the observed and 36-km REAM simulated vertical profiles on weekends.
411 Similar to Figures 3 and 5, observed and simulated concentrations of NO_2 are lower on weekends than on

https://doi.org/10.5194/acp-2020-1193
Preprint. Discussion started: 6 January 2021


Atmospheric Chemistry and Physics Discussions

412 weekdays. Some of the variations from weekend profiles are due to a lower number of observations (47 spirals)
413 on weekends. The overall agreement between the observed vertical profiles and 36-km model results is good on
414 weekends (R^2 = 0.81). At 15:00 – 17:00 LT, the model simulates a larger gradient than what the combination of
415 aircraft and surface measurements indicates. It may be related to the somewhat underestimated PBLHs in the late
416 afternoon in the model (Figure 4).

417 On weekdays, most simulated vertical profiles at the 4-km resolution (Figure 6e) are similar to 36-km results
418 in part because the average NO_x emissions over the six P-3B spiral sites are about the same, 4% lower in the 4-
419 km than the 36-km REAM simulations (Table S1). A clear exception is the 4-km REAM simulated vertical
420 profile at 15:00 – 17:00 LT when the model greatly overestimates boundary layer NO_x mixing and
421 concentrations. The main reason is that WRF simulated vertical velocities (*w*) in the late afternoon are much
422 larger in the 4-km simulation than the 36-km simulation (Figure S11), which can explain the simulated fully
423 mixed boundary layer at 15:00 – 17:00 LT. Since it is not designed to run at the 4-km resolution and it is
424 commonly assumed that convection can be resolved explicitly at high resolutions, the convection scheme is not
425 used in the nested 4-km WRF simulation (Table S2); it may be related to the large vertical velocities in the late
426 afternoon when thermal instability is the strongest. Appropriate convection parameterization is likely still
427 necessary for 4-km simulations (Zheng et al., 2016), which may also help alleviate the underestimation of
428 precipitation in the nested 4-km WRF simulation as discussed in section 2.1.

429 The same rapid boundary-layer mixing due to vertical transport is present in the 4-km REAM simulated
430 weekend vertical profile (Figure 6f), although the mixing height is lower. Fewer spirals (47) and distinct transport
431 effect due to different NO_2 horizontal gradients between the 4-km and 36-km REAM simulations (discussed in
432 detail in Section 3.5) may cause the overestimation of weekend profiles in the 4-km REAM simulation.

https://doi.org/10.5194/acp-2020-1193
Preprint. Discussion started: 6 January 2021


Atmospheric Chemistry and Physics Discussions

3.3 Daytime variation of NO_2 TVCDs

We compare satellite, P-3B aircraft, and model-simulated TVCDs with Pandora measurements, which provide continuous daytime observations. The locations of Pandora sites are shown in Table S1 and Figure S1. Among the Pandora sites, four sites are located significantly above the ground level: UMCP (~20 m), UMBC (~30 m), SERC (~40 m), and GSFC (~30 m). The other sites are 1.5 m AGL. To properly compare Pandora to other measurements and model simulations, we calculate the missing TVCDs between the Pandora site heights and ground surface by multiplying the Pandora TVCDs with model-simulated TVCD fractions of the corresponding columns. The resulting correction is 2-20% ($\frac{1}{1-missing\ TVCD\ percentage}$) for the four sites significantly above the ground surface, but the effect on the averaged daytime TVCD variation of all Pandora sites is small (Figure S14). In the following analysis, we use the updated Pandora TVCD data.

The weekday diurnal variations of NO_2 TVCDs from satellites, Pandora, 4- and 36-km REAM, and the P-3B aircraft are shown in Figure 7a. We calculate aircraft derived TVCDs by using equation (1):

$$TVCD_{aircraft}(t) = \frac{\sum c_{aircraft}(t) \times \rho_{REAM}(t) \times V_{REAM}(t)}{A_{REAM}} \quad (1),$$

where t is time; $c_{aircraft}$ (v/v) denotes aircraft NO_2 concentrations (mixing ratios) at each level at time t; ρ_{REAM} ($molecules\ /\ cm^3$) is the density of air from 36-km REAM at the corresponding level; V_{REAM} (cm^3) is the volume of the corresponding 36-km REAM grid cell; A_{REAM} (cm^2) is the surface area (36 × 36 km^2). In the calculation, we only use NO_2 concentrations below 3.63 km AGL because few aircraft measurements were available above this height in the campaign. Missing tropospheric NO_2 above 3.63 km AGL in the aircraft TVCD calculation has little impact on our analyses, as 36-km REAM model simulation shows that 85% ± 12% of tropospheric NO_2 are located below 3.63 km AGL during 6:00 – 17:00 LT in the DISCOVER-AQ region, which is roughly consistent with the GMI model results with 85% - 90% tropospheric NO_2 concentrated below 5 km (Lamsal et al., 2014). It

https://doi.org/10.5194/acp-2020-1193
Preprint. Discussion started: 6 January 2021


Atmospheric Chemistry and Physics Discussions

should be noted that only six P-3B spirals are available during the campaign, less than the samplings of 11 inland Pandora sites.

The 4-km REAM simulated NO_2 TVCDs are mostly higher than the 36-km results and the observations (Figure 7a). However, since the standard deviations of the data are much larger than the model difference, the 4- and 36-km model results show generally similar characteristics relative to the observations. REAM simulation results are in reasonable agreement with Pandora, P-3B aircraft, and satellite daytime NO_2 TVCDs, except that NASA-derived OMI (OMNO2) TVCDs are somewhat lower than other datasets, which may be partly due to biased a priori vertical profiles from the GMI model in the NASA retrieval in the campaign (Lamsal et al., 2014; Lamsal et al., 2020). TVCDs derived by using the DOMINO algorithm and 36-km REAM NO_2 vertical profiles are in agreement with those from KNMI, which indicates that the TM4 model from KNMI provides reasonable estimates of a priori NO_2 vertical profiles on weekdays in the DISCOVER-AQ region in summer.

We find evident decreases of NO_2 TVCDs from GOME-2A to OMI in Figure 7a, which is consistent with Pandora, REAM results, and previous studies that showed decreasing NO_2 TVCDs from SCIAMACHY to OMI due to photochemical losses in summer (Boersma et al., 2008; Boersma et al., 2009). P-3B aircraft TVCDs also show this decrease feature but have large variations due in part to the limited aircraft sampling data.

Pandora NO_2 TVCD data have different characteristics from REAM simulated and P-3B aircraft measured TVCDs at 5:00 – 7:00 LT and 14:00 – 18:00 LT (Figure 7a). At 5:00 – 7:00 LT, Pandora data show a significant increase of NO_2 TVCDs, but REAM and aircraft TVCDs decrease. At 14:00 LT – 18:00 LT, Pandora TVCDs have little variations, but REAM and aircraft TVCDs increase significantly. The relatively flat Pandora TVCDs in the late afternoon compared to REAM and P-3B aircraft measurements are consistent with Lamsal et al. (2017), which found the significant underestimation (26% – 30%) of Pandora VCDs compared to UC-12 ACAM

https://doi.org/10.5194/acp-2020-1193
Preprint. Discussion started: 6 January 2021


Atmospheric Chemistry and Physics Discussions

475 measurements from 16:00 LT to 18:00 LT during the DISCOVER-AQ campaign. We show the simulated effects
476 of emission, chemistry, transport, and dry deposition on NO_x TVCDs in Figure S13. The simulated early morning
477 decrease of NO_2 TVCDs is mainly due to the chemical transformation between NO_2 and NO favoring the
478 accumulation of NO under low-O_3 and low-HO_2/RO_2 conditions, thus NO TVCDs increase significantly but NO_2
479 TVCDs continue decreasing during the period. The increase in the late afternoon is primarily due to the decrease
480 of photochemistry-related sinks. The reasons for the discrepancies of NO_2 TVCDs between Pandora and REAM
481 results during the above two periods are unclear. Large SZAs in the early morning and the late afternoon (Figure
482 S8) lead to the higher uncertainties of Pandora measurements (Herman et al., 2009), although we have excluded
483 Pandora measurements with SZA > 80°. In addition, Pandora is a sun-tracking instrument with a small effective
484 FOV and is sensitive to local conditions within a narrow spatial range which may differ significantly from the
485 average properties of 36- and 4-km grid cells depending upon the time of the day (Figure S9) (Herman et al.,
486 2009; Herman et al., 2018; Herman et al., 2019; Judd et al., 2018; Judd et al., 2019; Judd et al., 2020; Lamsal et
487 al., 2017; Reed et al., 2015). Another possible reason is that Pandora instruments had few observations in the
488 early morning, and the resulting average may not be representative (Figure S9).

489 To further understand the daytime variation of NO_2 TVCDs, we examine P-3B aircraft data derived and
490 REAM simulated NO_2 VCD variations for different height bins (Figure 8). NO_2 VCDs below 3.63 km AGL
491 display a "U"-shaped pattern from 5:00 LT to 17:00 LT. In the morning, as vertical mixing becomes stronger
492 after sunrise, high-NO_x air in the lower layer is mixed with low-NO_x air in the upper layer. The increase of NO_x
493 vertical mixing above 400 m is sufficient to counter the increase of photochemical loss in the morning.
494 Conversely, the NO_2 VCDs below 400 m decrease remarkably from sunrise (about 6:00 LT) to around noontime
495 due to both vertical mixing and the increase of photochemical strength. From 13:00 LT to 16:00 LT, NO_2 VCDs
496 increase slowly, reflecting a relative balance among emissions, transport, chemistry, and dry depositions. The
497 sharp jump of the VCDs from 16:00 LT to 17:00 LT is mainly due to dramatically reduced chemical loss. And 4-

https://doi.org/10.5194/acp-2020-1193
Preprint. Discussion started: 6 January 2021


Atmospheric Chemistry and Physics Discussions

km REAM simulated NO_2 VCDs at 0.40-3.63 km at 16:00-17:00 LT are much higher than 36-km results because of the rapid vertical mixing in the 4-km REAM simulation (Figures 6 and S11).

Similar to NO_2 surface concentrations and vertical profiles in Figures 5 and 6, the NO_2 TVCD variation is also smaller on weekends than on weekdays, but the day-night pattern is similar (Figure 7). Although the 4-km REAM NO_2 TVCDs are generally higher than the 36-km results and observations in the daytime, considering their large standard deviations, NO_2 TVCDs from both simulations are comparable to satellite products, Pandora, and P-3B aircraft observations most of the time on weekends. The exception is that Pandora TVCDs have much less variation in the early morning and late afternoon than REAM simulation and aircraft datasets. Another anomaly is that KNMI GOME-2A TVCDs at 9:30 LT are much larger than the other datasets, while the GOME-2A TVCDs retrieved using 36-km REAM profiles shows comparable TVCDs to Pandora, REAM, and aircraft datasets, reflecting possible biased NO_2 a priori profiles from the TM4 model on weekends used in the KNMI GOME-2A retrieval.

3.4 Model comparisons with NO_y measurements

NO_y is longer-lived than NO_x, and NO_y concentrations are not affected by chemistry as much as NO_x. We obtain two types of NO_y concentrations from the P-3B aircraft in the DISCOVER-AQ campaign: one is NO_y concentrations directly measured by the NCAR 4-channel instrument, corresponding to the sum of NO, NO_2, $\sum$PNs, $\sum$ANs, HNO_3, N_2O_5, HNO_4, HONO, and the other reactive nitrogenic species in REAM (all the other species are described in Table 1); the other one, which we name as "derived-NO_y", is the sum of NO from the NCAR 4-channel instrument and NO_2 (NO_2_LIF), $\sum$PNs, $\sum$ANs, and HNO_3 measured by the TD-LIF technique, corresponding to NO, NO_2, $\sum$PNs, $\sum$ANs, and HNO_3 in REAM (Table 1). On average, P-3B derived-NO_y concentrations (2.88 ± 2.24 ppb) are 17% higher than coincident P-3B NO_y concentrations (2.46 ± 2.06 ppb) with $R^2 = 0.75$, generally reflecting consistency between these two types of measurements. As shown in Table 1, on

https://doi.org/10.5194/acp-2020-1193
Preprint. Discussion started: 6 January 2021


Atmospheric Chemistry and Physics Discussions

520 weekdays, the 36-km REAM NO_y concentrations are 45% larger than P-3B with R^2 = 0.33, and the 36-km
521 REAM derived-NO_y concentrations are 8% larger than P-3B with R^2 = 0.41. 4-km REAM show similar results,
522 suggesting that REAM simulations generally reproduce the observed NO_y and derived-NO_y concentrations within
523 the uncertainties, although the average values from REAM are somewhat larger than the observations. The
524 concentrations of weekday NO, NO_2, and ∑PNs from REAM simulations are also comparable to the
525 observations. However, weekday ∑ANs concentrations are 68% lower in the 36-km REAM than observations,
526 suggesting that the chemistry mechanism in REAM may need further improvement to better represent isoprene
527 nitrates. It is noteworthy that, since ∑ANs only account for a small fraction (~11%) in observed derived-NO_y, the
528 absolute difference between REAM simulated and P-3B observed ∑ANs concentrations is still small compared to
529 HNO_3. Weekday HNO_3 concentrations are significantly higher in REAM simulations (36-km: 57%, 0.65 ppb; 4-
530 km: 70%, 0.82 ppb) than P-3B observations, which is the main reason for the somewhat larger NO_y and derived-
531 NO_y concentrations in REAM compared to P-3B observations. The higher HNO_3 concentrations in REAM may
532 be related to the underestimation of precipitation in the corresponding WRF simulations, as discussed in section
533 2.1 (Figures S5), leading to the underestimated wet scavenging of HNO_3, especially for the 4-km REAM
534 simulation.

535 We also examine the weekday diurnal variations of derived-NO_y vertical profiles from P-3B and REAM
536 simulations in Figure S15. Generally, both 36- and 4-km REAM simulations capture the variation characteristics
537 of observed vertical profiles, which are similar to those for NO_2 in Figure 6. REAM derived-NO_y concentrations
538 are comparable to P-3B observations at most vertical levels on weekdays. Some larger derived-NO_y
539 concentrations in the model results can be partially explained by larger HNO_3 concentrations in REAM, such as
540 those below 1 km at 9:00 – 11:00 LT for the 36-km REAM and those below 2.0 km at 12:00 – 17:00 LT for the
541 4-km REAM (Figure S16).

https://doi.org/10.5194/acp-2020-1193
Preprint. Discussion started: 6 January 2021


Atmospheric Chemistry and Physics Discussions

Figure 9 shows the comparison of the diurnal cycles of surface NO_y concentrations observed at Padonia, Edgewood, Beltsville, and Aldino during the DISCOVER-AQ campaign with those from the REAM simulations. Generally, the REAM simulations reproduce the observed surface NO_y diurnal cycles except for the spikes around 17:00 – 20:00 LT due to still underestimated PBLHs (Figure 4). 4-km simulation results have a higher bias than 36-km results relative to the observations, similar to the comparisons of NO_2 surface concentrations and TVCDs in Figures 5 and 7 due to higher emissions around the observation sites in 4- than 36-km simulations (Table S1 and Figure S2).

3.5 Resolution dependence of NO_x emission distribution

We show previously that the 4-km REAM simulated NO_2 and NO_y surface concentrations and NO_2 TVCDs are higher than observations at daytime in comparison to the corresponding 36-km REAM results. An examination of monthly mean NO_2 surface concentrations and TVCDs for July 2011 also shows that 4-km simulation results are significantly higher than the 36-km results over the 11 inland Pandora sites in the daytime (Figure S17). The process-level diagnostics in Figure S13 indicate that the mean contribution of NO_x emissions to NO_x ΔTVCDs in the 4-km simulation is 1.32×10^{15} molecules cm^{-2} h^{-1} larger than that in the 36-km simulation between 9:00 LT and 16:00 LT, while the absolute mean contributions of chemistry and transport (they are negative in Figure S13, so we use absolute values here) in the 4-km simulation are 0.22×10^{15} and 0.99×10^{15} molecules cm^{-2} h^{-1} larger than the 36-km simulation, respectively. The contributions of dry deposition to NO_x ΔTVCDs are negligible compared to other factors in both simulations (Figure S13). Therefore, the 34% higher NO_x emissions over the 11 inland Pandora sites (Table S1 and Figure 1) is the main reason for the larger daytime NO_2 surface concentrations and TVCDs in the 4-km than the 36-km REAM simulations (Figure S17). The significantly different contribution changes between NO_x emissions (1.32×10^{15} molecules cm^{-2} h^{-1} or about one third) and chemistry (0.22×10^{15} molecules cm^{-2} h^{-1} or about 7%) reflect potential chemical nonlinearity (Li et al., 2019; Silvern et al., 2019; Valin et al., 2011) and transport effect. Different transport contributions between the 4-

https://doi.org/10.5194/acp-2020-1193
Preprint. Discussion started: 6 January 2021


Atmospheric Chemistry and Physics Discussions

565 km and the 36-km REAM are mainly caused by their different NO_x horizontal gradients (Figures S2 and 10),
566 while the impact of wind fields is small since we do not find significant differences in horizontal wind
567 components between the two simulations (Figure S18). The impact of transport on the two simulations can be
568 further verified by the comparison of NO_2 TVCDs over the six P-3B spiral sites between the two simulations
569 (Figure S19). Mean NO_x emissions over the six P-3B spiral sites are close (relative difference < 4%) between the
570 two simulations (Table S1 and Figure S19). From 9:00 to 12:00 LT, the contributions of NO_x emissions to NO_x
571 ΔTVCDs are 2.50×10^{15} and 2.49×10^{15} molecules cm^{-2} h^{-1} for the 36-km and 4-km REAM simulations,
572 respectively, and the contributions of chemistry are also close between the two simulations (36-km: -2.64×10^{15}
573 molecules cm^{-2} h^{-1}; 4-km: -2.68×10^{15} molecules cm^{-2} h^{-1}). However, the contributions of transport are $-0.32 \times$
574 10^{15} and 0.04×10^{15} molecules cm^{-2} h^{-1} for the 36-km and 4-km REAM simulations, respectively, leading to
575 larger NO_2 TVCDs in the 4-km REAM simulation than the 36-km REAM from 9:00 – 12:00 LT (Figure S19c).
576 Since horizontal wind fields over the six P-3B spiral sites are comparable between two simulations (Figures S3,
577 S4, and S18) and larger NO_x horizontal gradients are found near the P-3B spiral sites for the 4-km REAM (Figure
578 S2), we attribute the different transport contributions between the two simulations to a much larger NO_x emission
579 gradient around the measurement locations in 4-km than 36-km emission distributions.

580 We re-grid the 4-km REAM results into the grid cells of the 36-km REAM, which can significantly reduce
581 the impact of different NO_x emission distributions and associated transport on the two simulations. Compared to
582 the original 4-km REAM results, the re-gridded surface NO_2 concentrations and TVCDs over the 11 inland
583 Pandora sites are much closer to the 36-km REAM results (Figure S17). After re-gridding the 4-km REAM
584 results into 36-km REAM grid cells, we also find more comparable NO_y surface concentrations between the re-
585 gridded 4-km results and the 36-km REAM results (Figure S20). The remaining discrepancies between the re-
586 gridded results and the 36-km REAM results may be due to chemical nonlinearity and other meteorological
587 effects, such as larger vertical wind in the 4-km REAM (Figure S11) and their different k_{zz} values in the PBL.

https://doi.org/10.5194/acp-2020-1193
Preprint. Discussion started: 6 January 2021


Atmospheric Chemistry and Physics Discussions

Although other factors, such as chemical nonlinearity and vertical diffusion, may affect the 36-km and 4-km REAM simulations differently, the difference between 4- and 36-km simulations of reactive nitrogen is largely due to that of NO_x emissions.

The 4- and 36-km simulation difference depends on the location of the observations. In some regions, the NO_x emission difference between 4- and 36-km simulations is small. The comparison of NO_y measurements from P-3B spirals with coincident REAM results in Table 1 suggests that the 4-km and 36-km REAM simulations produce similar NO_y (relative difference ~2%) and derived-NO_y (relative difference ~4%) concentrations on weekdays, and both simulation results are comparable to the observations. The NO_y similarity over the P-3B spiral sites between the 36-km and 4-km REAM simulations is consistent with the comparable NO_x emissions over (relative difference < 4%) the six P-3B spiral sites between the two simulations (Table S1). The differences between the 4-km model simulation results and P3-B observations are larger on weekends than on weekdays (Table 1) due to the limited weekend sampling since model simulated monthly mean values show similar differences between the 4-km and 36-km REAM simulations on weekends as on weekdays (not shown).

3.6 Evaluation of 4-km NO_x distribution with ACAM measurements

The evaluation of model simulations of surface, aircraft, and satellite observations tends to point out a high bias in 4- than 36-km model simulations. However, we note that the uncertainties of the observations and model data are often comparable or larger than the model differences. Here we examine the 4-km model simulated NO_2 VCDs with high-resolution ACAM measurements onboard the UC-12 aircraft in Figures 10 and S21, respectively. The spatial distributions of ACAM and 4-km REAM NO_2 VCDs are generally consistent with R^2 = 0.37 on weekdays and R^2 = 0.50 on weekends. The domain averages of ACAM and 4-km REAM NO_2 VCDs are 4.7 ± 2.0 and 4.5 ± 3.2 × 10^{15} molecules cm^{-2} on weekdays and 3.0 ± 1.7 and 3.3 ± 2.8 × 10^{15} molecules cm^{-2} on weekends, respectively. The spatial distributions of ACAM and 4-km REAM NO_2 VCDs are highly correlated

https://doi.org/10.5194/acp-2020-1193
Preprint. Discussion started: 6 January 2021


Atmospheric Chemistry and Physics Discussions

610 with the spatial distribution of 4-km NEI2011 NO_x emissions. All three distributions capture two strong peaks
611 around Baltimore and Washington, D.C. urban regions and another weak peak in the northeast corner of the
612 domain (Wilmington city in Delaware) (Figures 10 and S21). However, Figures 10 and S21 clearly show that
613 NO_2 VCDs from the 4-km REAM simulation are more concentrated in Baltimore and Washington, D.C. urban
614 regions than ACAM, which are also reflected by the higher NO_2 VCD standard deviations of the 4-km REAM
615 results than ACAM. Several Pandora sites are in the highest NO_2 VCD regions where the 4-km REAM generally
616 produces larger NO_2 VCDs than ACAM, which explains why the NO_2 TVCDs over the 11 Pandora sites from the
617 4-km REAM simulation are higher than the observations (Figure 7) and the 36-km REAM results (Figure S17)
618 around noontime. Horizontal transport cannot explain the NO_2 VCD distribution biases in the 4-km REAM
619 simulation due to the following reasons. Firstly, horizontal wind fields are simulated as well by the nested 4-km
620 WRF simulation as the 36-km WRF compared to P-3B measurements, as discussed in section 2.1. Secondly, the
621 prevailing northwest wind in the daytime (Figure S4) should move NO_x eastward, but we find no significant
622 eastward shift of NO_2 VCDs compared to NO_x emissions in both ACAM and 4-km REAM distributions (Figure
623 10). Lastly, we find a local minimum of NO_2 VCDs in the middle of the Baltimore urban region (the purple circle
624 in Figure 10b) in the ACAM distribution, which cannot be explained by horizontal transport or chemical
625 nonlinearity due to the surrounding high NO_x emissions in the 4-km REAM simulation. Therefore, we attribute
626 the distribution inconsistency between ACAM and the 4-km REAM to the distribution biases of NEI2011 NO_x
627 emissions at the 4-km resolution since the average below-aircraft NO_2 VCDs between ACAM and the 4-km
628 REAM are about the same.

629 It is noteworthy that about 91% ACAM NO_2 VCD data are measured from 8:00 – 16:00 LT, and only using
630 ACAM NO_2 VCDs between 8:00 and 16:00 LT for the above comparison does not affect our results shown here.
631 Moreover, to minimize the effect of overestimated afternoon vertical mixing (Figure 6) on the 4-km REAM

https://doi.org/10.5194/acp-2020-1193
Preprint. Discussion started: 6 January 2021


Atmospheric Chemistry and Physics Discussions

632 simulation results, we also examine the comparison between ACAM NO_2 VCDs from 9:00 – 14:00 LT with
633 coincident 4-km REAM results, which produces similar results as shown here.

634 We also evaluate the NO_2 VCD distributions from the 4-km REAM simulation on weekdays and weekends
635 with ACAM NO_2 VCDs below the U-12 aircraft obtained from https://www-air.larc.nasa.gov/cgi-
636 bin/ArcView/discover-aq.dc-2011?UC12=1#LIU.XIONG/ in Figures S22 and S23. Although the domain mean
637 ACAM NO_2 VCDs in Figures S22 and S23 are higher than coincident 4-km REAM results due to the different
638 retrieval method from Lamsal et al. (2017), such as different above-aircraft NO_2 VCDs and different a priori NO_2
639 vertical profiles, we can still find clear distribution inconsistencies between the 4-km REAM and ACAM NO_2
640 VCDs. The 4-km REAM NO_2 VCDs are more concentrated in the Baltimore and Washington, D.C. urban regions
641 than this set of ACAM data, which is consistent with the conclusions derived from the ACAM dataset retrieved
642 by Lamsal et al. (2017).

643 3.7 Implications for NO_x emissions

644 The analysis of section 3.6 indicates that the NEI2011 NO_x emission distribution at the 4-km resolution is
645 likely biased for the Baltimore-Washington region. The distribution bias of the high-resolution NO_x emission
646 inventories is corroborated by the comparison of the NO_x emission inventory derived from the CONsolidated
647 Community Emissions Processor Tool, Motor Vehicle (CONCEPT MV) v2.1 with that estimated by the Sparse
648 Matrix Operator Kernel Emissions (SMOKE) v3.0 model with the Motor Vehicle Emissions Simulator (MOVES)
649 v2010a (DenBleyker et al., 2012). CONCEPT with finer vehicle activity information as input produced a wider-
650 spread but less-concentrated running exhaust NO_x emissions compared to MOVES in the Denver urban area for
651 July 2008 (DenBleyker et al., 2012). In addition, Canty et al. (2015) found that CMAQ 4.7.1, with on-road
652 emissions from MOVES and off-road emissions from the National Mobile Inventory Model (NMIM),
653 overestimated NO_2 TVCD over urban regions and underestimated NO_2 TVCDs over rural areas in the

https://doi.org/10.5194/acp-2020-1193
Preprint. Discussion started: 6 January 2021


Atmospheric Chemistry and Physics Discussions

654 northeastern U.S. for July and August 2011 compared to the OMNO2 product. The urban-rural contrast was also
655 found in Texas during the 2013 DISCOVER-AQ campaign in the studies of Souri et al. (2016) and Souri et al.
656 (2018), implying distribution uncertainties in NO_x emissions, although these studies and Canty et al. (2015)
657 focused more on polluted regions with overestimated NO_x emissions in their conclusions. The emission
658 distribution bias may also explain why Anderson et al. (2014) have different results from our simulated
659 concentrations in Table 1. In their study, they compared in-situ observations with a nested CMAQ simulation
660 with a resolution of 1.33 km. It is difficult to build up a reliable emission inventory for the whole U.S. at very
661 high resolutions with currently available datasets due to the significant inhomogeneity of NO_x emissions Marr et
662 al. (2013), but we can still expect significant improvements of the temporal-spatial distributions of NO_x
663 emissions in the near future as GPS-based information start to be used in the NEI estimates (DenBleyker et al.,
664 2017).

665 Although the NEI2011 NO_x emission distribution is likely biased at 4-km resolution, the similar average
666 below-aircraft NO_2 VCDs between ACAM and the 4-km REAM (Figure 10), as well as the good performance of
667 the 36-km REAM compared to NO_2 and NO_y observations (Figures 3 and 5-9 and Table 1), suggest that NEI2011
668 may provide reliable estimates of NO_x emissions over the Baltimore-Washington region at coarser resolutions. It
669 should be noted that although the good performance of the 36-km REAM in reproducing P-3B, Pandora, and
670 surface observations may be limited by representative errors due to the relatively coarse resolution of 36-km
671 REAM, ACAM and satellite NO_2 VCDs are all observations covering large areas, alleviating the problem caused
672 by observations limited to small areas. Our conclusion on the potential reliability of NEI2011 is consistent with
673 Salmon et al. (2018), who found NEI2011 and NEI2014 were in agreement with aircraft observation-derived NO_x
674 emissions during the Wintertime INvestigation of Transport, Emissions, and Reactivity (WINTER) campaign in
675 February – March 2015 around the Washington, D.C.-Baltimore area. The agreement was further confirmed
676 through the investigation of observed and NEI NO_x/CO_2, CO/NO_x, and CO/CO_2 ratios (Salmon et al., 2018).

https://doi.org/10.5194/acp-2020-1193
Preprint. Discussion started: 6 January 2021


Atmospheric Chemistry and Physics Discussions

677 However, our evaluation of NEI NO_x emissions is different from Travis et al. (2016) and Anderson et al. (2014).
678 Travis et al. (2016) compared the GEOS-Chem simulation results with the observations of NO_x and its oxidation
679 products from the SEAC^{4}RS campaign in the Southeast US, nitrate wet deposition fluxes from the National Acid
680 Deposition Program (NADP) network, and NO_2 TVCDs from OMI, and suggested that NEI2011 overestimated
681 mobile and industrial NO_x emissions by 30% – 60%. The GEOS-Chem chemical mechanism from Travis et al.
682 (2016) is almost the same as what we use in REAM, and their model simulation has a horizontal resolution of
683 0.25° × 0.3125°, which is also close to REAM (36 km × 36 km). We attribute the discrepancies between Travis et
684 al. (2016) and our study to the regional discrepancies. Travis et al. (2016) derived their conclusions based on the
685 averages of large domains (the whole CONUS or the Southeast U.S.), while our study focuses on the much
686 smaller Baltimore-Washington region. If limited to the Baltimore-Washington region, Figures 3 and 5 in Travis
687 et al. (2016) shown that nitrate wet deposition fluxes from NADP and TVCDs from the Berkeley High-
688 Resolution (BEHR) retrieval and NASA (OMNO2) were significantly higher than their simulations with NEI
689 non-power-plant NO_x emissions reduced by 60%, implying their conclusions about the overestimation of NEI
690 NO_x emissions at least not applicable to the Baltimore-Washington region. Anderson et al. (2014) evaluated
691 NEI2011 emissions with the observed concentration ratios of CO to NO_y and CO to NO_x from the same
692 DISCOVER-AQ campaign. They concluded that NEI overestimated NO_x emissions by 51% - 70% in Maryland
693 in the summer of 2011. However, the uncertainties of scaling the emission ratios of CO/NO_x to the concentrations
694 ratios of CO/NO_y or CO/NO_x can be large due in part to the large contribution of biogenic isoprene oxidation to
695 the variation of CO (Cheng et al., 2017). Furthermore, base CMAQ-simulated ∑PNs (1.4 ppbv) and ∑ANs (0.96
696 ppbv) concentrations by Anderson et al. (2014) are 0.79 and 0.64 ppbv higher than the corresponding P-3B
697 observations, respectively, leading to the overestimation of NO_y in their model; these biases are much larger than
698 those (~0.2 ppbv) from our 36-km REAM simulation as shown in Table 1, possibly due to different chemical
699 mechanisms used by CMAQ and REAM. Another possible reason, as mentioned above, is that the base CMAQ

https://doi.org/10.5194/acp-2020-1193
Preprint. Discussion started: 6 January 2021


Atmospheric Chemistry and Physics Discussions

used by Anderson et al. (2014) has a horizontal resolution of 1.33 km, much higher than our REAM simulations; NO_x emission distribution may be a potential issue causing the overestimation of the base CMAQ results.

Here, we emphasize that our study is not necessarily contradictory to recent studies concerning the overestimation of NEI NO_x emissions (Anderson et al., 2014; Canty et al., 2015; McDonald et al., 2018; Souri et al., 2016; Souri et al., 2018; Travis et al., 2016). Different types of observations in different periods and locations are analyzed for various purposes. This study focuses more on the spatial distribution of NO_x emissions in NEI2011 at the 4-km resolution, while previous studies are concerned more about the NO_x emission magnitudes in highly polluted sites, although the spatial distribution issue was also mentioned in some of the studies. If we limit our analyses to those observations in Figures 5, 7, and 9 and the 4-km REAM, we would also conclude an overestimation of NEI NO_x emissions. In this study, through comprehensive evaluations of NO_2 and NO_y measurements at 36- and 4-km resolutions, we provide another possible explanation for the overestimation of high-resolution model results at polluted sites. Although our assessment of NEI2011 NO_x emissions at 36-km resolution is contingent upon potential representative errors, the further comparisons of below-aircraft NO_2 VCDs between the 4-km REAM and ACAM from Lamsal et al. (2017) suggest that total NO_x emissions seem accurate but the emission distribution seems biased in the 4-km NEI2011 in our defined domain (Figure 10). Considering the significant heterogeneity of NO_x emissions, different conclusions on NO_x emission biases may be made in other regions, but the spatial distribution of NO_x emissions is a critical factor in evaluating NO_x emissions and improving emission estimation models, which deserves more attention in future studies.

4 Conclusions

We investigate the diurnal cycles of surface NO_2 concentrations, NO_2 vertical profiles, and NO_2 TVCDs using REAM model simulations on the basis of the observations from air quality monitoring sites, aircraft, Pandora, OMI, and GOME-2A during the DISCOVER-AQ 2011 campaign. We find that WRF simulated

https://doi.org/10.5194/acp-2020-1193
Preprint. Discussion started: 6 January 2021


Atmospheric Chemistry and Physics Discussions

722 nighttime PBLHs are significantly lower than ELF lidar measurements. Increasing nighttime mixing from 18:00
723 – 5:00 LT in the REAM simulations, we significantly improve REAM simulations of nighttime surface NO_2 and
724 O_3 concentrations.

725 The REAM simulation reproduces well the observed diurnal cycles of surface NO_2 and NO_y concentrations,
726 NO_2 vertical profiles, and NO_2 TVCDs on weekdays. Observed NO_2 concentrations in the boundary layer and
727 TVCDs on weekends are significantly lower than on weekdays. By specifying a weekend to weekday NO_x
728 emission ratio of 2:3 and applying a less variable NO_x emission diurnal profile on weekends than weekdays,
729 REAM can simulate well the weekend observations. A few issues are also noted. First, Pandora TVCDs show
730 different variations from aircraft-derived and REAM-simulated TVCDs in the early morning and late afternoon,
731 which may be due to the uncertainties of Pandora measurements at large SZAs and the small effective FOV of
732 Pandora. Second, the weekday OMI NO_2 TVCDs derived by NASA are somewhat lower than the KNMI OMI
733 product, P-3B aircraft-derived TVCDs, Pandora, and REAM results; the difference may be caused by the a priori
734 vertical profiles used in the NASA retrieval. Lastly, the weekend OMI NO_2 TVCDs derived by KNMI are larger
735 than those from Pandora, P-3B aircraft, REAM, and the OMI retrieval with REAM NO_2 vertical profiles,
736 indicating a possible bias of the TM4 simulated a priori NO_2 vertical profiles in the weekend mornings during
737 DISCOVER-AQ 2011.

738 While a higher-resolution simulation is assumed to be superior at a priori, the large observation dataset
739 during DISCOVER-AQ 2011 offers the opportunity of a detailed comparison of 4-km and 36-km model
740 simulations. In general, the 4-km simulation results tend to have a high bias relate to the 36-km results in light of
741 the observations. We find two areas that have not been widely recognized for high-resolution model simulations.
742 The first is not using convection parameterization in high-resolution WRF simulations since convection can be
743 resolved explicitly and convection parameterizations are not designed for high-resolution simulations. We find

https://doi.org/10.5194/acp-2020-1193
Preprint. Discussion started: 6 January 2021


Atmospheric Chemistry and Physics Discussions

that 4-km WRF tends to overestimate boundary-layer mixing and vertical transport in the late afternoon, leading to a high model bias in simulated NO_2 vertical profiles compared to P-3B aircraft observations. The reasons for this late-afternoon bias in 4-km WRF simulations and model modifications to mitigate this bias need further studies.

A second issue is related to the spatial distribution of NO_x emissions in NEI2011. At 4-km, the grid cells over the 11 inland Pandora sites have 34% higher NO_x emissions than the 36-km grid cells. Consequently, 4-km REAM overestimates NO_2 concentrations and TVCDs than the observations. The 4-km grid cells over four surface NO_y measurement sites have about a factor of 2 higher NO_x emissions than the corresponding 36-km grid cells, leading to significantly overestimated NO_y concentrations in the 4-km REAM simulation compared to the observations. After we re-grid the 4-km NO_2 and NO_y results to the 36-km grid cells, the results of 4-km simulations are similar to the original 36-km simulations. The comparison of 4-km ACAM NO_2 VCD measurements from the UC-12 aircraft with coincident 4-km REAM results shows that 4-km REAM NO_2 VCDs are more concentrated in urban regions than the ACAM observations. Further model analysis indicates that the 4-km VCD discrepancies are due primarily to the distribution bias of 4-km NEI2011 NO_x emissions. At high resolutions, potential biases in the emission inventories are accentuated when model results are evaluated with the observations. Our results highlight the research need to improve the methodologies and datasets used in emission estimates at high resolutions.

Data availability

The DISCOVER-AQ 2011 campaign datasets are archived on https://www-air.larc.nasa.gov/cgi-bin/ArcView/discover-aq.dc-2011 (last access: March 6, 2020). EPA air quality monitoring datasets are from https://www3.epa.gov/airdata/ (last access: June 23, 2015). The NASA OMI NO_2 product is from https://disc.gsfc.nasa.gov/datasets/OMNO2_003/summary (last access: September 26, 2020). The KNMI OMI

https://doi.org/10.5194/acp-2020-1193
Preprint. Discussion started: 6 January 2021


Atmospheric Chemistry and Physics Discussions

766 NO_2 product is from http://www.temis.nl/airpollution/no2.html (last access: January 14, 2015). We obtain the
767 KNMI GOME-2A NO_2 VCD archives from http://www.temis.nl/airpollution/no2col/no2colgome2_v2.php (last
768 access: January 22, 2015). The GMI MERRA-2 simulation results are from
769 https://portal.nccs.nasa.gov/datashare/dirac/gmidata2/users/mrdamon/Hindcast-
770 Family/HindcastMR2/2011/stations/ (last access: May 14, 2019). We obtain the UC-12 ACAM NO_2 VCD
771 product by X. Liu from https://www-air.larc.nasa.gov/cgi-bin/ArcView/discover-aq.dc-
772 2011?UC12=1#LIU.XIONG/ (last access: December 31, 2019). The Stage IV precipitation data is downloaded
773 from https://rda.ucar.edu/datasets/ds507.5/ (last access: December 28, 2019). The NCEP CFSv2 6-hourly product
774 is available at http://rda.ucar.edu/datasets/ds094.0/ (last access: March 10, 2015). REAM simulation results for
775 this study and the UC-12 ACAM NO_2 VCD product by Lamsal et al. (2017) are available upon request.

776 **Author contribution**

777 JL and YW designed the study. JL, RZ, and CS updated the REAM model. JL conducted model simulations.
778 KFB developed the DOMINO algorithm, CS applied the algorithm to REAM vertical profiles, and JL updated the
779 retrieval algorithm and did the retrieval by using REAM NO_2 vertical profiles. AW, JH, EAC, RWL, JJS, RD,
780 AMT, TNK, LNL, SJJ, MGK, XL, CRN made various measurements in the DISCOVER-AQ 2011 campaign. JL
781 conducted the analyses with discussions with YW, RZ, CS, AW, JH, KFB, EAC, RWL, JJS, RD, AMT, TNK,
782 LNL, SJJ, MGK, XL, and CRN. JL and YW led the writing of the manuscript with inputs from all other
783 coauthors. All coauthors reviewed the manuscript.

784 **Competing interests**

785 The authors declare that they have no conflict of interest.

https://doi.org/10.5194/acp-2020-1193
Preprint. Discussion started: 6 January 2021


Atmospheric Chemistry and Physics Discussions

Acknowledgments

This work was supported by the NASA ACMAP Program. We thank Chun Zhao for providing us the PNNL NEI2011 emission inventory. We thank Yuzhong Zhang and Jenny Fisher for providing the updated GEOS-Chem chemistry mechanism files and thank Yuzhong Zhang, Yongjia Song, Hang Qu, Ye Cheng, Aoxing Zhang, Yufei Zou and Ziming Ke for discussion with J. Li. We thank Susan Strahan for providing the GMI outputs download link.

References

Anderson, D. C., Loughner, C. P., Diskin, G., Weinheimer, A., Canty, T. P., Salawitch, R. J., Worden, H. M., Fried, A., Mikoviny, T., and Wisthaler, A.: Measured and modeled CO and NO_y in DISCOVER-AQ: An evaluation of emissions and chemistry over the eastern US, Atmos. Environ., 96, 78-87, https://doi.org/10.1016/j.atmosenv.2014.07.004, 2014.

Beirle, S., Platt, U., Wenig, M., and Wagner, T.: Weekly cycle of NO_2 by GOME measurements: A signature of anthropogenic sources, Atmos. Chem. Phys., 3, 2225-2232, https://doi.org/10.5194/acp-3-2225-2003, 2003.

Boersma, K. F., Eskes, H. J., Veefkind, J. P., Brinksma, E. J., Van Der A, R. J., Sneep, M., Van Den Oord, G. H. J., Levelt, P. F., Stammes, P., and Gleason, J. F.: Near-real time retrieval of tropospheric NO_2 from OMI, Atmos. Chem. Phys., 7, 2103-2118, https://doi.org/10.5194/acp-7-2103-2007, 2007.

Boersma, K. F., Jacob, D. J., Eskes, H. J., Pinder, R. W., Wang, J., and Van Der A, R. J.: Intercomparison of SCIAMACHY and OMI tropospheric NO_2 columns: Observing the diurnal evolution of chemistry and emissions from space, J. Geophys. Res.-Atmos., 113, https://doi.org/10.1029/2007JD008816, 2008.

Boersma, K. F., Jacob, D. J., Trainic, M., Rudich, Y., De Smedt, I., Dirksen, R., and Eskes, H. J.: Validation of urban NO_2 concentrations and their diurnal and seasonal variations observed from the SCIAMACHY and OMI sensors using in situ surface measurements in Israeli cities, Atmos. Chem. Phys., 9, 3867-3879, https://doi.org/10.5194/acp-9-3867-2009, 2009.

Boersma, K. F., Eskes, H. J., Dirksen, R. J., Veefkind, J. P., Stammes, P., Huijnen, V., Kleipool, Q. L., Sneep, M., Claas, J., and Leitão, J.: An improved tropospheric NO_2 column retrieval algorithm for the Ozone Monitoring Instrument, Atmos. Meas. Tech., 4, 1905-1928, https://doi.org/10.5194/amt-4-1905-2011, 2011.

Boersma, K. F., Eskes, H. J., Richter, A., De Smedt, I., Lorente, A., Beirle, S., van Geffen, J. H., Zara, M., Peters, E., and Roozendael, M. V.: Improving algorithms and uncertainty estimates for satellite NO_2 retrievals: results from the quality assurance for the essential climate variables (QA4ECV) project, Atmos. Meas. Tech., 11, 6651-6678, https://doi.org/10.5194/amt-11-6651-2018, 2018.

816 Breuer, H., Ács, F., Horváth, Á., Németh, P., and Rajkai, K.: Diurnal course analysis of the WRF-simulated and
817 observation-based planetary boundary layer height, Advances in Science and Research, 11, 83-88,
818 https://doi.org/10.5194/asr-11-83-2014, 2014.

819 Brohede, S., McLinden, C. A., Berthet, G., Haley, C. S., Murtagh, D., and Sioris, C. E.: A stratospheric NO_2
820 climatology from Odin/OSIRIS limb-scatter measurements, Can. J. Phys., 85, 1253-1274,
821 https://doi.org/10.1139/p07-141, 2007.

822 Brown, S. S., Dibb, J. E., Stark, H., Aldener, M., Vozella, M., Whitlow, S., Williams, E. J., Lerner, B. M.,
823 Jakoubek, R., and Middlebrook, A. M.: Nighttime removal of NO_x in the summer marine boundary layer,
824 Geophys. Res. Lett., 31, https://doi.org/10.1029/2004GL019412, 2004.

825 Bucsela, E. J., Krotkov, N. A., Celarier, E. A., Lamsal, L. N., Swartz, W. H., Bhartia, P. K., Boersma, K. F.,
826 Veefkind, J. P., Gleason, J. F., and Pickering, K. E.: A new stratospheric and tropospheric NO_2 retrieval
827 algorithm for nadir-viewing satellite instruments: applications to OMI, Atmos. Meas. Tech., 6, 2607-2626,
828 https://doi.org/10.5194/amt-6-2607-2013, 2013.

829 Canty, T., Hembeck, L., Vinciguerra, T., Goldberg, D., Carpenter, S., Allen, D., Loughner, C., Salawitch, R., and
830 Dickerson, R.: Ozone and NO_x chemistry in the eastern US: evaluation of CMAQ/CB05 with satellite (OMI)
831 data, Atmos. Chem. Phys., 15, 10965, https://doi.org/10.5194/acp-15-10965-2015, 2015.

832 Chance, K.: OMI Algorithm Theoretical Basis Document: OMI Trace Gas Algorithms, available at
833 https://ozoneaq.gsfc.nasa.gov/media/docs/ATBD-OMI-04.pdf, Smithsonian Astrophysical Observatory,
834 Cambridge, MA, USA2.0, 78, 2002.

835 Cheng, Y., Wang, Y., Zhang, Y., Chen, G., Crawford, J. H., Kleb, M. M., Diskin, G. S., and Weinheimer, A. J.:
836 Large biogenic contribution to boundary layer O_3-CO regression slope in summer, Geophys. Res. Lett., 44, 7061-
837 7068, https://doi.org/10.1002/2017GL074405, 2017.

838 Cheng, Y., Wang, Y., Zhang, Y., Crawford, J. H., Diskin, G. S., Weinheimer, A. J., and Fried, A.: Estimator of
839 surface ozone using formaldehyde and carbon monoxide concentrations over the eastern United States in
840 summer, J. Geophys. Res.-Atmos., 123, 7642-7655, https://doi.org/10.1029/2018JD028452, 2018.

841 Choi, S., Lamsal, L. N., Follette-Cook, M., Joiner, J., Krotkov, N. A., Swartz, W. H., Pickering, K. E., Loughner,
842 C. P., Appel, W., Pfister, G., Saide, P. E., Cohen, R. C., Weinheimer, A. J., and Herman, J. R.: Assessment of
843 NO_2 observations during DISCOVER-AQ and KORUS-AQ field campaigns, Atmos. Meas. Tech., 13, 2523-
844 2546, https://doi.org/10.5194/amt-13-2523-2020, 2020.

845 Choi, Y., Wang, Y., Zeng, T., Cunnold, D., Yang, E. S., Martin, R., Chance, K., Thouret, V., and Edgerton, E.:
846 Springtime transitions of NO_2, CO, and O_3 over North America: Model evaluation and analysis, J. Geophys.
847 Res.-Atmos., 113, https://doi.org/10.1029/2007JD009632, 2008.

848 Choi, Y., Kim, H., Tong, D., and Lee, P.: Summertime weekly cycles of observed and modeled NO_x and O_3
849 concentrations as a function of satellite-derived ozone production sensitivity and land use types over the
850 Continental United States, Atmos. Chem. Phys., 12, 6291-6307, https://doi.org/10.5194/acp-12-6291-2012, 2012.

Compton, J. C., Delgado, R., Berkoff, T. A., and Hoff, R. M.: Determination of planetary boundary layer height on short spatial and temporal scales: A demonstration of the covariance wavelet transform in ground-based wind profiler and lidar measurements, Journal of Atmospheric and Oceanic Technology, 30, 1566-1575, https://doi.org/10.1175/JTECH-D-12-00116.1, 2013.

David, L. M., and Nair, P. R.: Diurnal and seasonal variability of surface ozone and NO_x at a tropical coastal site: Association with mesoscale and synoptic meteorological conditions, J. Geophys. Res.-Atmos., 116, https://doi.org/10.1029/2010JD015076, 2011.

Davis, C., Brown, B., and Bullock, R.: Object-based verification of precipitation forecasts. Part I: Methodology and application to mesoscale rain areas, Monthly Weather Review, 134, 1772-1784, https://doi.org/10.1175/MWR3145.1, 2006.

Day, D. A., Wooldridge, P. J., Dillon, M. B., Thornton, J. A., and Cohen, R. C.: A thermal dissociation laser - induced fluorescence instrument for in situ detection of NO_2, peroxy nitrates, alkyl nitrates, and HNO_3, J. Geophys. Res.-Atmos., 107, ACH 4-1-ACH 4-14, https://doi.org/10.1029/2001JD000779, 2002.

de Foy, B.: City-level variations in NOx emissions derived from hourly monitoring data in Chicago, Atmos. Environ., 176, 128-139, https://doi.org/10.1016/j.atmosenv.2017.12.028, 2018.

DenBleyker, A., Morris, R. E., Lindhjem, C. E., Parker, L. K., Shah, T., Koo, B., Loomis, C., and Dilly, J.: Temporal and Spatial Detail in Mobile Source Emission Inventories for Regional Air Quality Modeling, 2012 International Emission Inventory Conference, Florida, U.S., August 13 - 16, 2012, 2012.

DenBleyker, A., Koupal, J., DeFries, T., and Palacios, C.: Improvement of Default Inputs for MOVES and SMOKE-MOVES: CRC Project A-100, available at https://crcao.org/reports/recentstudies2017/A-100/ERG_FinalReport_CRCA100_28Feb2017.pdf, Eastern Research Group, Inc., Austin, TX, 86, 2017.

Dirksen, R. J., Boersma, K. F., Eskes, H. J., Ionov, D. V., Bucsela, E. J., Levelt, P. F., and Kelder, H. M.: Evaluation of stratospheric NO_2 retrieved from the Ozone Monitoring Instrument: Intercomparison, diurnal cycle, and trending, J. Geophys. Res.-Atmos., 116, https://doi.org/10.1029/2010JD014943, 2011.

EPA: Profile of the 2011 National Air Emissions Inventory, available at https://www.epa.gov/sites/production/files/2015-08/documents/lite_finalversion_ver10.pdf, U.S. Environmental Protection Agency, 2014.

Fisher, J. A., Jacob, D. J., Travis, K. R., Kim, P. S., Marais, E. A., Chan Miller, C., Yu, K., Zhu, L., Yantosca, R. M., and Sulprizio, M. P.: Organic nitrate chemistry and its implications for nitrogen budgets in an isoprene-and monoterpene-rich atmosphere: constraints from aircraft ($SEAC^4RS$) and ground-based (SOAS) observations in the Southeast US, Atmos. Chem. Phys., 16, 5969-5991, https://doi.org/10.5194/acp-16-5969-2016, 2016.

Flynn, C. M., Pickering, K. E., Crawford, J. H., Lamsal, L., Krotkov, N., Herman, J., Weinheimer, A., Chen, G., Liu, X., and Szykman, J.: Relationship between column-density and surface mixing ratio: Statistical analysis of O_3 and NO_2 data from the July 2011 Maryland DISCOVER-AQ mission, Atmos. Environ., 92, 429-441, https://doi.org/10.1016/j.atmosenv.2014.04.041, 2014.

886 Frey, M. M., Brough, N., France, J. L., Anderson, P. S., Traulle, O., King, M. D., Jones, A. E., Wolff, E. W., and
887 Savarino, J.: The diurnal variability of atmospheric nitrogen oxides (NO and NO_2) above the Antarctic Plateau
888 driven by atmospheric stability and snow emissions, Atmos. Chem. Phys., 13, 3045-3062,
889 https://doi.org/10.5194/acp-13-3045-2013, 2013.

890 Gaur, A., Tripathi, S. N., Kanawade, V. P., Tare, V., and Shukla, S. P.: Four-year measurements of trace gases
891 (SO_2, NO_x, CO, and O_3) at an urban location, Kanpur, in Northern India, Journal of Atmospheric Chemistry, 71,
892 283-301, https://doi.org/10.1007/s10874-014-9295-8, 2014.

893 Gourley, J. J., Hong, Y., Flamig, Z. L., Wang, J., Vergara, H., and Anagnostou, E. N.: Hydrologic evaluation of
894 rainfall estimates from radar, satellite, gauge, and combinations on Ft. Cobb basin, Oklahoma, Journal of
895 Hydrometeorology, 12, 973-988, https://doi.org/10.1175/2011JHM1287.1, 2011.

896 Guenther, A. B., Jiang, X., Heald, C. L., Sakulyanontvittaya, T., Duhl, T., Emmons, L. K., and Wang, X.: The
897 Model of Emissions of Gases and Aerosols from Nature version 2.1 (MEGAN2.1): an extended and updated
898 framework for modeling biogenic emissions, Geosci. Model Dev., 5, 1471-1492, https://doi.org/10.5194/gmd-5-
899 1471-2012, 2012.

900 Hains, J. C., Boersma, K. F., Kroon, M., Dirksen, R. J., Cohen, R. C., Perring, A. E., Bucsela, E., Volten, H.,
901 Swart, D. P. J., and Richter, A.: Testing and improving OMI DOMINO tropospheric NO_2 using observations
902 from the DANDELIONS and INTEX - B validation campaigns, J. Geophys. Res.-Atmos., 115,
903 https://doi.org/10.1029/2009JD012399, 2010.

904 Herman, J., Cede, A., Spinei, E., Mount, G., Tzortziou, M., and Abuhassan, N.: NO_2 column amounts from
905 ground-based Pandora and MFDOAS spectrometers using the direct-Sun DOAS technique: Intercomparisons and
906 application to OMI validation, J. Geophys. Res.-Atmos., 114, https://doi.org/10.1029/2009JD011848, 2009.

907 Herman, J., Spinei, E., Fried, A., Kim, J., Kim, J., Kim, W., Cede, A., Abuhassan, N., and Segal-Rozenhaimer,
908 M.: NO_2 and HCHO measurements in Korea from 2012 to 2016 from Pandora spectrometer instruments
909 compared with OMI retrievals and with aircraft measurements during the KORUS-AQ campaign, Atmos. Meas.
910 Tech., 11, 4583-4603, https://doi.org/10.5194/amt-11-4583-2018, 2018.

911 Herman, J., Abuhassan, N., Kim, J., Kim, J., Dubey, M., Raponi, M., and Tzortziou, M.: Underestimation of
912 column NO_2 amounts from the OMI satellite compared to diurnally varying ground-based retrievals from
913 multiple PANDORA spectrometer instruments, Atmos. Meas. Tech., 12, 5593-5612, https://doi.org/10.5194/amt-
914 12-5593-2019, 2019.

915 Hu, X., Doughty, D. C., Sanchez, K. J., Joseph, E., and Fuentes, J. D.: Ozone variability in the atmospheric
916 boundary layer in Maryland and its implications for vertical transport model, Atmos. Environ., 46, 354-364,
917 https://doi.org/10.1016/j.atmosenv.2011.09.054, 2012.

918 Huijnen, V., Eskes, H. J., Poupkou, A., Elbern, H., Boersma, K. F., Foret, G., Sofiev, M., Valdebenito, A.,
919 Flemming, J., and Stein, O.: Comparison of OMI NO_2 tropospheric columns with an ensemble of global and
920 European regional air quality models, Atmos. Chem. Phys., 10, 3273-3296, https://doi.org/10.5194/acp-10-3273-
921 2010, 2010.

Ionov, D. V., Timofeyev, Y. M., Sinyakov, V. P., Semenov, V. K., Goutail, F., Pommereau, J. P., Bucsela, E. J., Celarier, E. A., and Kroon, M.: Ground‐based validation of EOS‐Aura OMI NO_2 vertical column data in the midlatitude mountain ranges of Tien Shan (Kyrgyzstan) and Alps (France), J. Geophys. Res.-Atmos., 113, https://doi.org/10.1029/2007JD008659, 2008.

Irie, H., Kanaya, Y., Akimoto, H., Tanimoto, H., Wang, Z., Gleason, J. F., and Bucsela, E. J.: Validation of OMI tropospheric NO_2 column data using MAX-DOAS measurements deep inside the North China Plain in June 2006: Mount Tai Experiment 2006, Atmos. Chem. Phys., 8, 6577-6586, https://doi.org/10.5194/acp-8-6577-2008, 2008.

Irie, H., Boersma, K. F., Kanaya, Y., Takashima, H., Pan, X., and Wang, Z.: Quantitative bias estimates for tropospheric NO_2 columns retrieved from SCIAMACHY, OMI, and GOME-2 using a common standard for East Asia, Atmos. Meas. Tech., 5, 2403-2411, https://doi.org/10.5194/amt-5-2403-2012, 2012.

Jones, A. E., Weller, R., Wolff, E. W., and Jacobi, H. W.: Speciation and rate of photochemical NO and NO_2 production in Antarctic snow, Geophys. Res. Lett., 27, 345-348, https://doi.org/10.1029/1999GL010885, 2000.

Judd, L. M., Al-Saadi, J. A., Valin, L. C., Pierce, R. B., Yang, K., Janz, S. J., Kowalewski, M. G., Szykman, J. J., Tiefengraber, M., and Mueller, M.: The Dawn of Geostationary Air Quality Monitoring: Case Studies from Seoul and Los Angeles, Front. Environ. Sci., 6, 85, https://doi.org/10.3389/fenvs.2018.00085, 2018.

Judd, L. M., Al-Saadi, J. A., Janz, S. J., Kowalewski, M. G., Pierce, R. B., Szykman, J. J., Valin, L. C., Swap, R., Cede, A., Mueller, M., Tiefengraber, M., Abuhassan, N., and Williams, D.: Evaluating the impact of spatial resolution on tropospheric NO_2 column comparisons within urban areas using high-resolution airborne data, Atmos. Meas. Tech., 12, 6091-6111, https://doi.org/10.5194/amt-12-6091-2019, 2019.

Judd, L. M., Al-Saadi, J. A., Szykman, J. J., Valin, L. C., Janz, S. J., Kowalewski, M. G., Eskes, H. J., Veefkind, J. P., Cede, A., Mueller, M., Gebetsberger, M., Swap, R., Pierce, R. B., Nowlan, C. R., Abad, G. G., Nehrir, A., and Williams, D.: Evaluating Sentinel-5P TROPOMI tropospheric NO_2 column densities with airborne and Pandora spectrometers near New York City and Long Island Sound, Atmos. Meas. Tech. Discuss., 2020, 1-52, https://doi.org/10.5194/amt-2020-151, 2020.

Kalinga, O. A., and Gan, T. Y.: Estimation of rainfall from infrared‐microwave satellite data for basin‐scale hydrologic modelling, Hydrological processes, 24, 2068-2086, https://doi.org/10.1002/hyp.7626, 2010.

Kaynak, B., Hu, Y., Martin, R. V., Sioris, C. E., and Russell, A. G.: Comparison of weekly cycle of NO_2 satellite retrievals and NO_x emission inventories for the continental United States, J. Geophys. Res.-Atmos., 114, https://doi.org/10.1029/2008JD010714, 2009.

Kim, S. W., McDonald, B., Baidar, S., Brown, S., Dube, B., Ferrare, R., Frost, G., Harley, R., Holloway, J., and Lee, H. J.: Modeling the weekly cycle of NO_x and CO emissions and their impacts on O_3 in the Los Angeles-South Coast Air Basin during the CalNex 2010 field campaign, J. Geophys. Res.-Atmos., 121, 1340-1360, https://doi.org/10.1002/2015JD024292, 2016.

Knepp, T., Pippin, M., Crawford, J., Chen, G., Szykman, J., Long, R., Cowen, L., Cede, A., Abuhassan, N., and Herman, J.: Estimating surface NO_2 and SO_2 mixing ratios from fast-response total column observations and potential application to geostationary missions, Journal of atmospheric chemistry, 72, 261-286, https://doi.org/10.1007/s10874-013-9257-6, 2015.

Krotkov, N. A., Lamsal, L. N., Celarier, E. A., Swartz, W. H., Marchenko, S. V., Bucsela, E. J., Chan, K. L., Wenig, M., and Zara, M.: The version 3 OMI NO_2 standard product, Atmos. Meas. Tech., 10, 3133-3149, https://doi.org/10.5194/amt-10-3133-2017, 2017.

Lamsal, L. N., Krotkov, N. A., Celarier, E. A., Swartz, W. H., Pickering, K. E., Bucsela, E. J., Gleason, J. F., Martin, R. V., Philip, S., and Irie, H.: Evaluation of OMI operational standard NO_2 column retrievals using in situ and surface-based NO_2 observations, Atmos. Chem. Phys., 14, 11587-11609, https://doi.org/10.5194/acp-14-11587-2014, 2014.

Lamsal, L. N., Duncan, B. N., Yoshida, Y., Krotkov, N. A., Pickering, K. E., Streets, D. G., and Lu, Z.: US NO_2 trends (2005–2013): EPA Air Quality System (AQS) data versus improved observations from the Ozone Monitoring Instrument (OMI), Atmos. Environ., 110, 130-143, https://doi.org/10.1016/j.atmosenv.2015.03.055, 2015.

Lamsal, L. N., Janz, S. J., Krotkov, N. A., Pickering, K. E., Spurr, R. J. D., Kowalewski, M. G., Loughner, C. P., Crawford, J. H., Swartz, W. H., and Herman, J.: High‐resolution NO_2 observations from the Airborne Compact Atmospheric Mapper: Retrieval and validation, J. Geophys. Res.-Atmos., 122, 1953-1970, https://doi.org/10.1002/2016JD025483, 2017.

Lamsal, L. N., Krotkov, N. A., Vasilkov, A., Marchenko, S., Qin, W., Yang, E. S., Fasnacht, Z., Joiner, J., Choi, S., Haffner, D., Swartz, W. H., Fisher, B., and Bucsela, E.: OMI/Aura Nitrogen Dioxide Standard Product with Improved Surface and Cloud Treatments, Atmos. Meas. Tech. Discuss., 2020, 1-56, https://doi.org/10.5194/amt-2020-200, 2020.

Levelt, P. F., Hilsenrath, E., Leppelmeier, G. W., van den Oord, G. H. J., Bhartia, P. K., Tamminen, J., de Haan, J. F., and Veefkind, J. P.: Science objectives of the ozone monitoring instrument, IEEE Transactions on Geoscience and Remote Sensing, 44, 1199-1208, https://doi.org/10.1109/TGRS.2006.872336, 2006.

Li, J., Wang, Y., and Qu, H.: Dependence of summertime surface ozone on NO_x and VOC emissions over the United States: Peak time and value, Geophys. Res. Lett., 46, 3540-3550, https://doi.org/10.1029/2018GL081823, 2019.

Li, J., Feng, Z., Qian, Y., and Leung, L. R.: A high-resolution unified observational data product of mesoscale convective systems and isolated deep convection in the United States for 2004-2017, Earth Syst. Sci. Data Discuss., 2020, 1-48, https://doi.org/10.5194/essd-2020-151, 2020.

Lin, Y., and Mitchell, K. E.: 1.2 the NCEP stage II/IV hourly precipitation analyses: Development and applications, 19th Conf. Hydrology, American Meteorological Society, San Diego, CA, USA, 2005,

990 Liu, C., Liu, X., Kowalewski, M., Janz, S., González Abad, G., Pickering, K., Chance, K., and Lamsal, L.:
991 Analysis of ACAM data for trace gas retrievals during the 2011 DISCOVER-AQ campaign, Journal of
992 Spectroscopy, 2015, https://doi.org/10.1155/2015/827160, 2015a.

993 Liu, C., Liu, X., Kowalewski, M. G., Janz, S. J., González Abad, G., Pickering, K. E., Chance, K., and Lamsal, L.
994 N.: Characterization and verification of ACAM slit functions for trace-gas retrievals during the 2011
995 DISCOVER-AQ flight campaign, Atmos. Meas. Tech., 8, 751-759, https://doi.org/10.5194/amt-8-751-2015,
996 2015b.

997 Liu, Z., Wang, Y., Gu, D., Zhao, C., Huey, L. G., Stickel, R., Liao, J., Shao, M., Zhu, T., and Zeng, L.:
998 Summertime photochemistry during CAREBeijing-2007: RO_x budgets and O_3 formation, Atmos. Chem. Phys.,
999 12, 7737-7752, https://doi.org/10.5194/acp-12-7737-2012, 2012.

1000 Lopez, P.: Direct 4D-Var assimilation of NCEP stage IV radar and gauge precipitation data at ECMWF, Monthly
1001 Weather Review, 139, 2098-2116, https://doi.org/10.1175/2010MWR3565.1, 2011.

1002 Luo, G., Yu, F., and Schwab, J.: Revised treatment of wet scavenging processes dramatically improves GEOS-
1003 Chem 12.0.0 simulations of surface nitric acid, nitrate, and ammonium over the United States, Geosci. Model
1004 Dev., 12, 3439-3447, https://doi.org/10.5194/gmd-12-3439-2019, 2019.

1005 Marchenko, S., Krotkov, N., Lamsal, L., Celarier, E., Swartz, W., and Bucsela, E.: Revising the slant column
1006 density retrieval of nitrogen dioxide observed by the Ozone Monitoring Instrument, J. Geophys. Res.-Atmos.,
1007 120, 5670-5692, https://doi.org/10.1002/2014JD022913, 2015.

1008 Marr, L. C., Moore, T. O., Klapmeyer, M. E., and Killar, M. B.: Comparison of NO_x Fluxes Measured by Eddy
1009 Covariance to Emission Inventories and Land Use, Environ. Sci. Technol., 47, 1800-1808,
1010 https://doi.org/10.1021/es303150y, 2013.

1011 McDonald, B., McKeen, S., Cui, Y. Y., Ahmadov, R., Kim, S.-W., Frost, G. J., Pollack, I., Peischl, J., Ryerson,
1012 T. B., and Holloway, J.: Modeling Ozone in the Eastern US using a Fuel-Based Mobile Source Emissions
1013 Inventory, Environ. Sci. Technol., https://doi.org/10.1021/acs.est.8b00778, 2018.

1014 Munro, R., Eisinger, M., Anderson, C., Callies, J., Corpaccioli, E., Lang, R., Lefebvre, A., Livschitz, Y., and
1015 Albinana, A. P.: GOME-2 on MetOp, Proc. of The 2006 EUMETSAT Meteorological Satellite Conference,
1016 Helsinki, Finland, 2006, 48,

1017 Nelson, B. R., Prat, O. P., Seo, D.-J., and Habib, E.: Assessment and implications of NCEP Stage IV quantitative
1018 precipitation estimates for product intercomparisons, Weather and Forecasting, 31, 371-394,
1019 https://doi.org/10.1175/WAF-D-14-00112.1, 2016.

1020 Ng, N. L., Brown, S. S., Archibald, A. T., Atlas, E., Cohen, R. C., Crowley, J. N., Day, D. A., Donahue, N. M.,
1021 Fry, J. L., and Fuchs, H.: Nitrate radicals and biogenic volatile organic compounds: oxidation, mechanisms, and
1022 organic aerosol, Atmos. Chem. Phys., 17, 2103-2162, https://doi.org/10.5194/acp-17-2103-2017, 2017.

1023 Nowlan, C. R., Liu, X., Leitch, J. W., Chance, K., González Abad, G., Liu, C., Zoogman, P., Cole, J., Delker, T.,
1024 Good, W., Murcray, F., Ruppert, L., Soo, D., Follette-Cook, M. B., Janz, S. J., Kowalewski, M. G., Loughner, C.
1025 P., Pickering, K. E., Herman, J. R., Beaver, M. R., Long, R. W., Szykman, J. J., Judd, L. M., Kelley, P., Luke, W.
1026 T., Ren, X., and Al-Saadi, J. A.: Nitrogen dioxide observations from the Geostationary Trace gas and Aerosol
1027 Sensor Optimization (GeoTASO) airborne instrument: Retrieval algorithm and measurements during
1028 DISCOVER-AQ Texas 2013, Atmos. Meas. Tech., 9, 2647-2668, https://doi.org/10.5194/amt-9-2647-2016,
1029 2016.

1030 Nowlan, C. R., Liu, X., Janz, S. J., Kowalewski, M. G., Chance, K., Follette-Cook, M. B., Fried, A., González
1031 Abad, G., Herman, J. R., Judd, L. M., Kwon, H. A., Loughner, C. P., Pickering, K. E., Richter, D., Spinei, E.,
1032 Walega, J., Weibring, P., and Weinheimer, A. J.: Nitrogen dioxide and formaldehyde measurements from the
1033 GEOstationary Coastal and Air Pollution Events (GEO-CAPE) Airborne Simulator over Houston, Texas, Atmos.
1034 Meas. Tech., 11, 5941-5964, https://doi.org/10.5194/amt-11-5941-2018, 2018.

1035 Oetjen, H., Baidar, S., Krotkov, N. A., Lamsal, L. N., Lechner, M., and Volkamer, R.: Airborne MAX-DOAS
1036 measurements over California: Testing the NASA OMI tropospheric NO_2 product, J. Geophys. Res.-Atmos., 118,
1037 7400-7413, https://doi.org/10.1002/jgrd.50550, 2013.

1038 Peng, J., Hu, M., Guo, S., Du, Z., Zheng, J., Shang, D., Zamora, M. L., Zeng, L., Shao, M., and Wu, Y.-S.:
1039 Markedly enhanced absorption and direct radiative forcing of black carbon under polluted urban environments,
1040 Proc. Natl. Acad. Sci. U.S.A., 201602310, https://doi.org/10.1073/pnas.1602310113, 2016.

1041 Peters, E., Wittrock, F., Großmann, K., Frieß, U., Richter, A., and Burrows, J. P.: Formaldehyde and nitrogen
1042 dioxide over the remote western Pacific Ocean: SCIAMACHY and GOME-2 validation using ship-based MAX-
1043 DOAS observations, Atmos. Chem. Phys., 12, 11179-11197, https://doi.org/10.5194/acp-12-11179-2012, 2012.

1044 Reddy, B. S. K., Kumar, K. R., Balakrishnaiah, G., Gopal, K. R., Reddy, R. R., Sivakumar, V., Lingaswamy, A.
1045 P., Arafath, S. M., Umadevi, K., and Kumari, S. P.: Analysis of diurnal and seasonal behavior of surface ozone
1046 and its precursors (NO_x) at a semi-arid rural site in Southern India, Aerosol Air Qual Res, 12, 1081-1094,
1047 https://doi.org/10.4209/aaqr.2012.03.0055 2012.

1048 Reed, A. J., Thompson, A. M., Kollonige, D. E., Martins, D. K., Tzortziou, M. A., Herman, J. R., Berkoff, T. A.,
1049 Abuhassan, N. K., and Cede, A.: Effects of local meteorology and aerosols on ozone and nitrogen dioxide
1050 retrievals from OMI and pandora spectrometers in Maryland, USA during DISCOVER-AQ 2011, Journal of
1051 atmospheric chemistry, 72, 455-482, https://doi.org/10.1007/s10874-013-9254-9, 2015.

1052 Reed, C., Evans, M. J., Carlo, P. D., Lee, J. D., and Carpenter, L. J.: Interferences in photolytic NO_2
1053 measurements: explanation for an apparent missing oxidant?, Atmos. Chem. Phys., 16, 4707-4724,
1054 https://doi.org/10.5194/acp-16-4707-2016, 2016.

1055 Richter, A., Begoin, M., Hilboll, A., and Burrows, J. P.: An improved NO_2 retrieval for the GOME-2 satellite
1056 instrument, Atmos. Meas. Tech., 4, 1147-1159, https://doi.org/10.5194/amt-4-1147-2011, 2011.

1057 Russell, A. R., Valin, L. C., and Cohen, R. C.: Trends in OMI NO_2 observations over the United States: effects of
1058 emission control technology and the economic recession, Atmos. Chem. Phys., 12, 12197-12209,
1059 https://doi.org/10.5194/acp-12-12197-2012, 2012.

1060 Saha, S., Moorthi, S., Wu, X., Wang, J., Nadiga, S., Tripp, P., Behringer, D., Hou, Y. T., Chuang, H.-y., and
1061 Iredell, M.: NCEP climate forecast system version 2 (CFSv2) 6-hourly products, available at
1062 https://rda.ucar.edu/datasets/ds094.0/, https://doi.org/10.5065/D61C1TXF, 2011 (last access: Mar 10, 2015).

1063 Salmon, O., Shepson, P., Ren, X., He, H., Hall, D., Dickerson, R., Stirm, B., Brown, S., Fibiger, D., and
1064 McDuffie, E.: Top‐down Estimates of NO_x and CO Emissions from Washington, DC‐Baltimore During the
1065 WINTER Campaign, J. Geophys. Res.-Atmos., https://doi.org/10.1029/2018JD028539, 2018.

1066 Sawamura, P., Müller, D., Hoff, R. M., Hostetler, C. A., Ferrare, R. A., Hair, J. W., Rogers, R. R., Anderson, B.
1067 E., Ziemba, L. D., and Beyersdorf, A. J.: Aerosol optical and microphysical retrievals from a hybrid
1068 multiwavelength lidar data set–DISCOVER-AQ 2011, Atmos. Meas. Tech., 7, 3095-3112,
1069 https://doi.org/10.5194/amt-7-3095-2014, 2014.

1070 Seinfeld, J. H., and Pandis, S. N.: Atmospheric chemistry and physics: from air pollution to climate change, John
1071 Wiley & Sons, Inc, Hoboken, New Jersey, 2016.

1072 Sen, B., Toon, G. C., Osterman, G. B., Blavier, J.-F., Margitan, J. J., Salawitch, R. J., and Yue, G. K.:
1073 Measurements of reactive nitrogen in the stratosphere, J. Geophys. Res.-Atmos., 103, 3571-3585,
1074 https://doi.org/10.1029/97JD02468, 1998.

1075 Shin, H. H., and Hong, S.-Y.: Intercomparison of planetary boundary-layer parametrizations in the WRF model
1076 for a single day from CASES-99, Boundary-Layer Meteorology, 139, 261-281, https://doi.org/10.1007/s10546-
1077 010-9583-z, 2011.

1078 Silvern, R. F., Jacob, D. J., Mickley, L. J., Sulprizio, M. P., Travis, K. R., Marais, E. A., Cohen, R. C., Laughner,
1079 J. L., Choi, S., Joiner, J., and Lamsal, L. N.: Using satellite observations of tropospheric NO_2 columns to infer
1080 long-term trends in US NO_x emissions: the importance of accounting for the free tropospheric NO_2 background,
1081 Atmos. Chem. Phys., 19, 8863-8878, https://doi.org/10.5194/acp-19-8863-2019, 2019.

1082 Souri, A. H., Choi, Y., Jeon, W., Li, X., Pan, S., Diao, L., and Westenbarger, D. A.: Constraining NO_x emissions
1083 using satellite NO_2 measurements during 2013 DISCOVER-AQ Texas campaign, Atmos. Environ., 131, 371-
1084 381, https://doi.org/10.1016/j.atmosenv.2016.02.020, 2016.

1085 Souri, A. H., Choi, Y., Pan, S., Curci, G., Nowlan, C. R., Janz, S. J., Kowalewski, M. G., Liu, J., Herman, J. R.,
1086 and Weinheimer, A. J.: First top‐down estimates of anthropogenic NO_x emissions using high‐resolution
1087 airborne remote sensing observations, J. Geophys. Res.-Atmos., 123, 3269-3284,
1088 https://doi.org/10.1002/2017JD028009, 2018.

1089 Spinei, E., Cede, A., Swartz, W. H., Herman, J., and Mount, G. H.: The use of NO_2 absorption cross section
1090 temperature sensitivity to derive NO_2 profile temperature and stratospheric–tropospheric column partitioning

1091 from visible direct-sun DOAS measurements, Atmos. Meas. Tech., 7, 4299-4316, https://doi.org/10.5194/amt-7-
1092 4299-2014, 2014.

1093 Spurr, R.: LIDORT and VLIDORT: Linearized pseudo-spherical scalar and vector discrete ordinate radiative
1094 transfer models for use in remote sensing retrieval problems, in: Light Scattering Reviews 3, Springer, 229-275,
1095 2008.

1096 Thornton, J. A., Wooldridge, P. J., and Cohen, R. C.: Atmospheric NO_2: In situ laser-induced fluorescence
1097 detection at parts per trillion mixing ratios, Anal. Chem., 72, 528-539, https://doi.org/10.1021/ac9908905, 2000.

1098 Tong, D., Lamsal, L., Pan, L., Ding, C., Kim, H., Lee, P., Chai, T., Pickering, K. E., and Stajner, I.: Long-term
1099 NO_x trends over large cities in the United States during the great recession: Comparison of satellite retrievals,
1100 ground observations, and emission inventories, Atmos. Environ., 107, 70-84,
1101 https://doi.org/10.1016/j.atmosenv.2015.01.035, 2015.

1102 Travis, K. R., Jacob, D. J., Fisher, J. A., Kim, P. S., Marais, E. A., Zhu, L., Yu, K., Miller, C. C., Yantosca, R.
1103 M., and Sulprizio, M. P.: Why do models overestimate surface ozone in the Southeast United States?, Atmos.
1104 Chem. Phys., 16, 13561-13577, https://doi.org/10.5194/acp-16-13561-2016, 2016.

1105 Tu, J., Xia, Z.-G., Wang, H., and Li, W.: Temporal variations in surface ozone and its precursors and
1106 meteorological effects at an urban site in China, Atmospheric Research, 85, 310-337,
1107 https://doi.org/10.1016/j.atmosres.2007.02.003, 2007.

1108 Valin, L. C., Russell, A. R., Hudman, R. C., and Cohen, R. C.: Effects of model resolution on the interpretation
1109 of satellite NO_2 observations, Atmos. Chem. Phys., 11, 11647-11655, https://doi.org/10.5194/acp-11-11647-
1110 2011, 2011.

1111 van der A, R. J., Eskes, H. J., Roozendael, M. V., De Smedt, I., Blond, N., Boersma, F., Weiss, A., and van Peet,
1112 J. C. A.: Algorithm Document Tropospheric NO_2, available at http://www.temis.nl/docs/AD_NO2.pdf1.0, 23,
1113 2010.

1114 Van Geffen, J., Boersma, K., Van Roozendael, M., Hendrick, F., Mahieu, E., De Smedt, I., Sneep, M., and
1115 Veefkind, J.: Improved spectral fitting of nitrogen dioxide from OMI in the 405–465 nm window, Atmos. Meas.
1116 Tech., 8, 1685-1699, https://doi.org/10.5194/amt-8-1685-2015, 2015.

1117 Van Stratum, B. J. H., Vilà-Guerau de Arellano, J., Ouwersloot, H. G., Dries, K. d., Van Laar, T. W., Martinez,
1118 M., Lelieveld, J., Diesch, J.-M., Drewnick, F., and Fischer, H.: Case study of the diurnal variability of chemically
1119 active species with respect to boundary layer dynamics during DOMINO, Atmos. Chem. Phys., 12, 5329-5341,
1120 https://doi.org/10.5194/acp-12-5329-2012, 2012.

1121 Wooldridge, P. J., Perring, A. E., Bertram, T. H., Flocke, F. M., Roberts, J. M., Singh, H. B., Huey, L. G.,
1122 Thornton, J. A., Wolfe, G. M., and Murphy, J. G.: Total Peroxy Nitrates ([Sigma] PNs) in the atmosphere: the
1123 Thermal Dissociation-Laser Induced Fluorescence (TD-LIF) technique and comparisons to speciated PAN
1124 measurements, Atmos. Meas. Tech., 3, 593, https://doi.org/10.5194/amt-3-593-2010, 2010.

1125 Yuan, H., McGinley, J. A., Schultz, P. J., Anderson, C. J., and Lu, C.: Short-range precipitation forecasts from
1126 time-lagged multimodel ensembles during the HMT-West-2006 campaign, Journal of Hydrometeorology, 9, 477-
1127 491, https://doi.org/10.1175/2007JHM879.1, 2008.

1128 Zhang, R., Wang, Y., Smeltzer, C., Qu, H., Koshak, W., and Boersma, K. F.: Comparing OMI-based and EPA
1129 AQS in situ NO_2 trends: towards understanding surface NO_x emission changes, Atmos. Meas. Tech., 11, 3955-
1130 3967, https://doi.org/10.5194/amt-11-3955-2018, 2018.

1131 Zhang, Y., and Wang, Y.: Climate-driven ground-level ozone extreme in the fall over the Southeast United
1132 States, Proc. Natl. Acad. Sci. U.S.A., 113, 10025-10030, https://doi.org/10.1073/pnas.1602563113, 2016.

1133 Zhang, Y., Wang, Y., Chen, G., Smeltzer, C., Crawford, J., Olson, J., Szykman, J., Weinheimer, A. J., Knapp, D.
1134 J., and Montzka, D. D.: Large vertical gradient of reactive nitrogen oxides in the boundary layer: Modeling
1135 analysis of DISCOVER‐AQ 2011 observations, J. Geophys. Res.-Atmos., 121, 1922-1934,
1136 https://doi.org/10.1002/2015JD024203, 2016.

1137 Zhao, C., Wang, Y., Choi, Y., and Zeng, T.: Summertime impact of convective transport and lightning NO_x
1138 production over North America: modeling dependence on meteorological simulations, Atmos. Chem. Phys., 9,
1139 4315-4327, https://doi.org/10.5194/acp-9-4315-2009, 2009.

1140 Zheng, Y., Alapaty, K., Herwehe, J. A., Del Genio, A. D., and Niyogi, D.: Improving high-resolution weather
1141 forecasts using the Weather Research and Forecasting (WRF) Model with an updated Kain–Fritsch scheme,
1142 Monthly Weather Review, 144, 833-860, https://doi.org/10.1175/MWR-D-15-0005.1, 2016.

1143

Table 1. Comparison of the concentrations of NO_y and its components between REAM and P-3B aircraft measurements during the DISCOVER-AQ campaign

			NO_y / ppb[1]	NO / ppb	NO_2_NCAR / ppb	NO_2_LIF / ppb[2]	∑PNs / ppb	∑ANs / ppb	HNO_3 / ppb	Derived-NO_y / ppb[3]
36-km[4]	Weekday[5]	P-3B	2.51 ± 2.09	0.18 ± 0.29	0.85 ± 1.13	0.68 ± 0.95	0.70 ± 0.58	0.31 ± 0.23	1.15 ± 0.73	2.86 ± 2.26
		REAM	3.64 ± 3.15	0.18 ± 0.31	0.74 ± 1.06	0.68 ± 0.90	0.53 ± 0.45	0.10 ± 0.09	1.80 ± 1.62	3.10 ± 2.71
		R^2	0.33	0.33	0.37	0.33	0.37	0.38	0.24	0.41
	Weekend	P-3B	3.01 ± 2.19	0.15 ± 0.20	0.71 ± 0.80	0.63 ± 0.72	0.91 ± 0.53	0.36 ± 0.21	1.15 ± 0.79	2.96 ± 2.15
		REAM	3.76 ± 2.24	0.15 ± 0.17	0.53 ± 0.61	0.53 ± 0.60	0.52 ± 0.29	0.09 ± 0.06	2.30 ± 1.40	3.41 ± 2.30
		R^2	0.29	0.28	0.41	0.45	0.27	0.38	0.49	0.51
4-km	Weekday	P-3B	2.51 ± 2.15	0.19 ± 0.30	0.85 ± 1.29	0.67 ± 0.96	0.70 ± 0.59	0.31 ± 0.22	1.17 ± 0.74	2.90 ± 2.27
		REAM	3.67 ± 3.63	0.17 ± 0.29	0.74 ± 1.12	0.72 ± 1.10	0.45 ± 0.51	0.08 ± 0.10	1.99 ± 1.92	3.23 ± 3.24
		R^2	0.25	0.46	0.48	0.55	0.37	0.27	0.60	0.44
	Weekend	P-3B	2.97 ± 2.13	0.15 ± 0.18	0.69 ± 0.75	0.65 ± 0.85	0.90 ± 0.51	0.35 ± 0.21	1.15 ± 0.79	2.93 ± 2.08
		REAM	4.22 ± 3.79	0.24 ± 0.42	0.83 ± 1.40	0.78 ± 1.34	0.38 ± 0.27	0.07 ± 0.08	2.48 ±2.04	3.59 ± 3.59
		R^2	0.20	0.33	0.37	0.30	0.15	0.20	0.59	0.35

[1] For P-3B, the concentrations of NO_y, NO, and NO_2_NCAR were measured by using the NCAR 4-channel chemiluminescence instrument. The measurement uncertainties are 10%, 10 - 15%, and 10% for NO, NO_2, and NO_y, respectively. The 1-second, 1-sigma detection limits are 20 pptv, 30 pptv, and 20 pptv for NO, NO_2, and NO_y, respectively (https://discover-aq.larc.nasa.gov/pdf/2010STM/Weinheimer20101005_DISCOVERAQ_AJW.pdf). For REAM, NO_y is the sum of NO, NO_2, total peroxyacyl nitrates (∑PNs), total alkyl nitrates (∑ANs) (include alkyl nitrates and hydroxyalkyl nitrates), HNO_3, HONO, 2 × N_2O_5, HNO_4, first generation C5 carbonyl nitrate (nighttime isoprene nitrate ISN1: $C_5H_8NO_4$), 2 × C5 dihydroxydinitrate (DHDN: $C_5H_{10}O_8N_2$), methyl peroxy nitrate (MPN: $CH_3O_2NO_2$), propanone nitrate (PROPNN: $CH_3C(=O)CH_2ONO_2$), nitrate from methyl vinyl ketone (MVKN: $HOCH_2CH(ONO_2)C(=O)CH_3$), nitrate from methacrolein (MARCN: $HOCH_2C(ONO_2)(CH_3)CHO$), and ethanol nitrate (ETHLN: $CHOCH_2ONO_2$).

[2] For P-3B, the concentrations of NO_2_LIF, ∑PNs, ∑ANs, and HNO_3 were measured by applying the thermal dissociation-laser induced fluorescence (TD-LIF) technique. The accuracy of TD-LIF measurements of NO_2, ∑PNs, ∑ANs, and HNO_3 is better than 15%, and the detection limit for the sum of NO_2, ∑PNs, ∑ANs, and HNO_3 is ~ 10 ppt 10 s^{-1} (Day et al., 2002).

[3] To compare NO_y concentrations from TD-LIF measurements with those from REAM, we calculate derived-NO_y as the sum of NO, NO_2_LIF, ∑PNs, ∑ANs, and HNO_3. Only when the concentrations of all the five species are available at the same hour in the same grid cell, we can calculate derived-NO_y at the given hour in the given grid cell. Therefore, in Table 1, the averaged derived-NO_y values are not exactly equal to the sum of averaged NO, NO_2_LIF, ∑PNs, ∑ANs, and HNO_3 concentrations that only depend on the availability of a single species. In addition, the measurement times and frequencies between NO_y and derived-NO_y are not the same. A comparison between these two types of data needs coincident sampling, as described in the main text.

[4] Mean NO_x emissions over the six P-3B spiral sites are close (relative difference < 4%) between the 36-km and 4-km REAM (Table S1).

[5] Due to different sampling times and locations between weekdays and weekends, we do not recommend a direct comparison between weekday and weekend values here.

Atmospheric Chemistry and Physics Discussions
Open Access
EGU

https://doi.org/10.5194/acp-2020-1193
Preprint. Discussion started: 6 January 2021

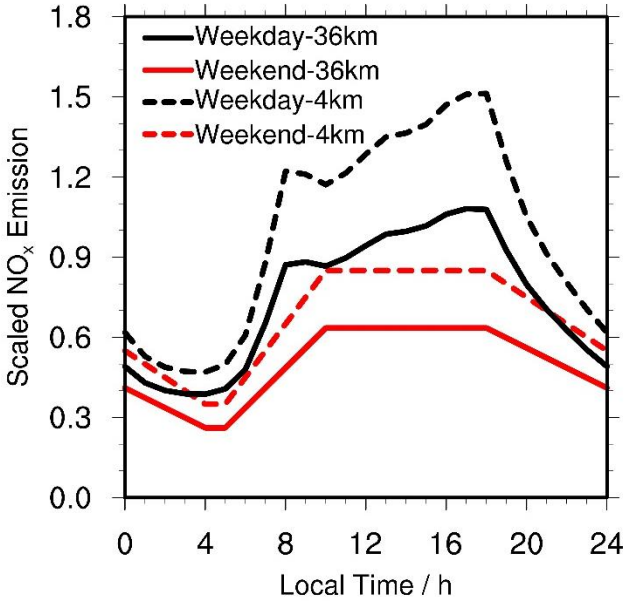

Figure 1. Relative diurnal profiles of weekday and weekend NO_x emissions (molecules km^{-2} s^{-1}) in the DISCOVER-AQ 2011 region (the 36/4 km grid cells over the 11 inland Pandora sites shown in Figure S1) for the 36-km and 4-km REAM. All the profiles are scaled by the 4-km weekday emission average value (molecules km^{-2} s^{-1}).

https://doi.org/10.5194/acp-2020-1193
Preprint. Discussion started: 6 January 2021

Atmospheric Chemistry and Physics Discussions

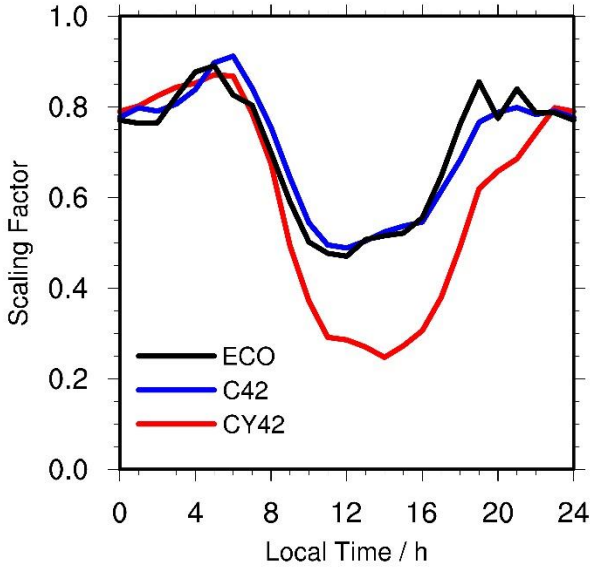

Figure 2. Hourly ratios of NO_2 measurements from the Teledyne API model 200 eup photolytic NO_x analyzer to NO_2 from coincident catalytic instruments for 2011 July. "CY42" denotes the ratios of photolytic NO_2 to NO_2 from the Thermo Electron 42C-Y NO_y analyzer in Edgewood, "C42" denotes the ratios of photolytic NO_2 to NO_2 from the Thermo Model 42C NO_x analyzer in Padonia, and "ECO" denotes the ratios of photolytic NO_2 to NO_2 from the Ecotech Model 9841 T-NO_y analyzer in Padonia. "ECO" ratios are also used to scale NO_2 measurements from the Ecotech Model 9843 T-NO_y analyzer. Thermo Model 42I-Y NO_y analyzer was used only in Padonia, where photolytic measurements were available, so we do not use the Thermo Model 42I-Y NO_y analyzer measurements in this study.

https://doi.org/10.5194/acp-2020-1193
Preprint. Discussion started: 6 January 2021

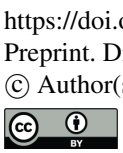

Atmospheric Chemistry and Physics Discussions

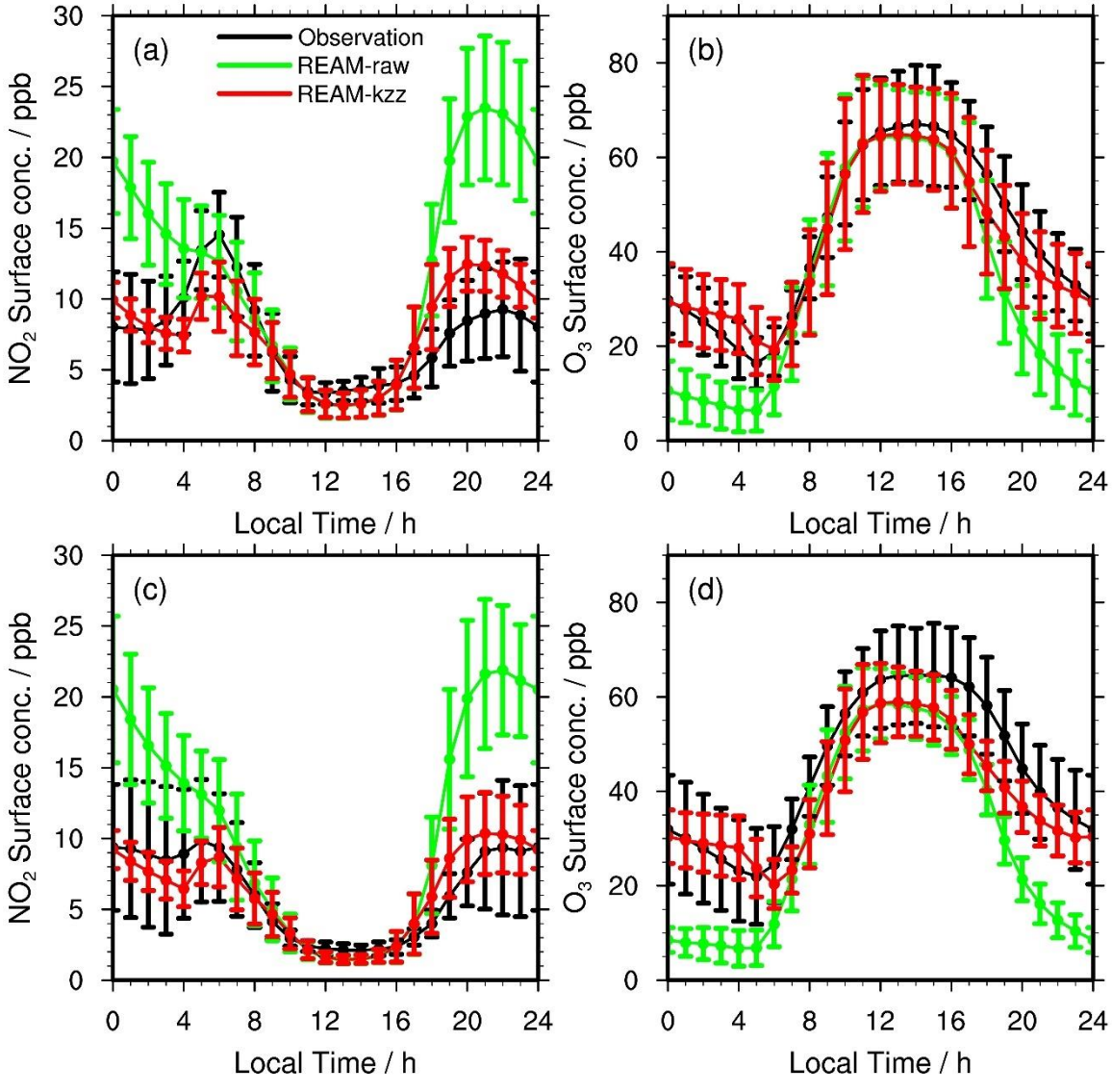

Figure 3. Diurnal cycles of surface (a, c) NO_2 and (b, d) O_3 concentrations on (a, b) weekdays and (c, d) weekends during the DISCOVER-AQ campaign in the DISCOVER-AQ region (the 36-km grid cells over the 11 inland Pandora sites shown in Figure S1). Black lines denote the mean observations from all the 11 NO_2 surface monitoring sites and 19 O_3 surface sites during the campaign (Figure S1), as mentioned in Section 2.5. "REAM-raw" (green lines) denotes the coincident 36-km REAM simulation results with WRF simulated k_{zz} data, and "REAM-kzz" (red lines) is the coincident 36-km REAM simulation results with updated k_{zz} data. See the main text for details. Vertical bars denote corresponding standard deviations.

https://doi.org/10.5194/acp-2020-1193
Preprint. Discussion started: 6 January 2021

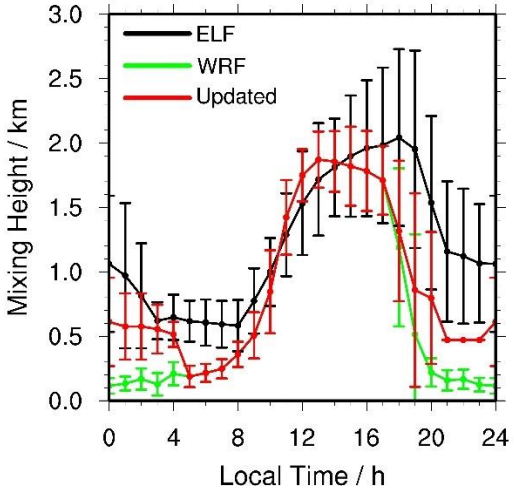

Figure 4. ELF observed and model simulated diurnal variations of PBLH at the UMBC site during the Discover-AQ campaign. "ELF" denotes ELF derived PBLHs by using the covariance wavelet transform method. "WRF" denotes the 36-km WRF k_{zz}-determined PBLHs, and "Updated" denotes updated k_{zz}-determined PBLHs. See the main text for details. Vertical bars denote standard deviations.

https://doi.org/10.5194/acp-2020-1193
Preprint. Discussion started: 6 January 2021

Atmospheric Chemistry and Physics Discussions

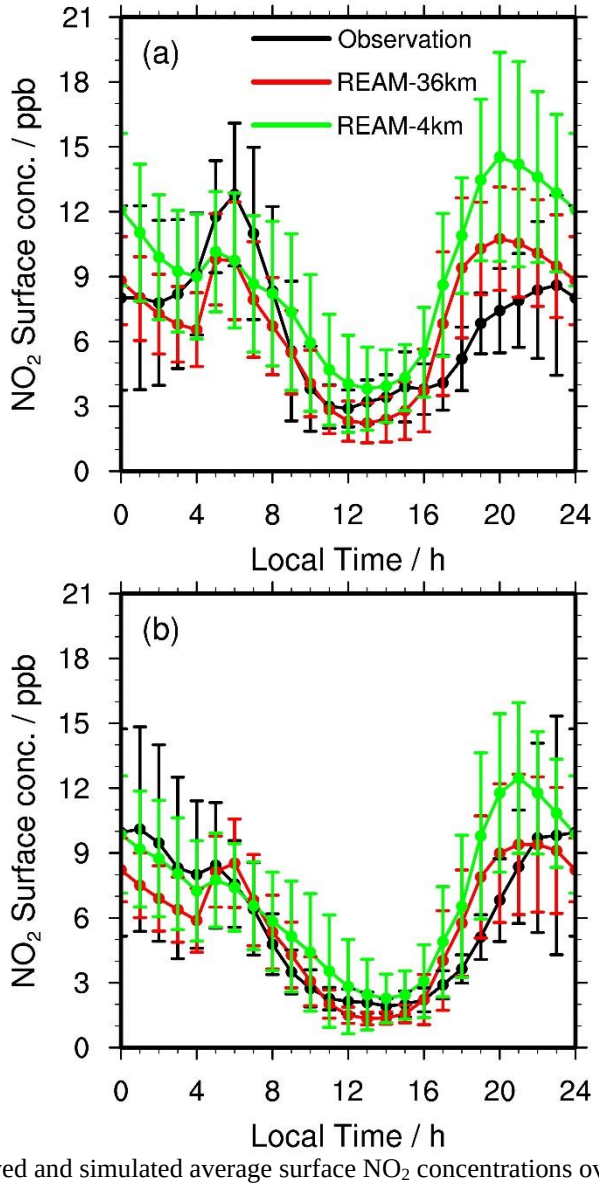

Figure 5. Diurnal cycles of observed and simulated average surface NO_2 concentrations over Padonia, Oldtown, Essex, Edgewood, Beltsville, and Aldino (Table S1) on (a) weekdays and (b) weekends. Black lines denote mean observations from the six sites. Red lines denote coincident 36-km REAM simulation results, and green lines are for coincident 4-km REAM simulation results. Error bars denote standard deviations.

https://doi.org/10.5194/acp-2020-1193
Preprint. Discussion started: 6 January 2021

Atmospheric Chemistry and Physics Discussions

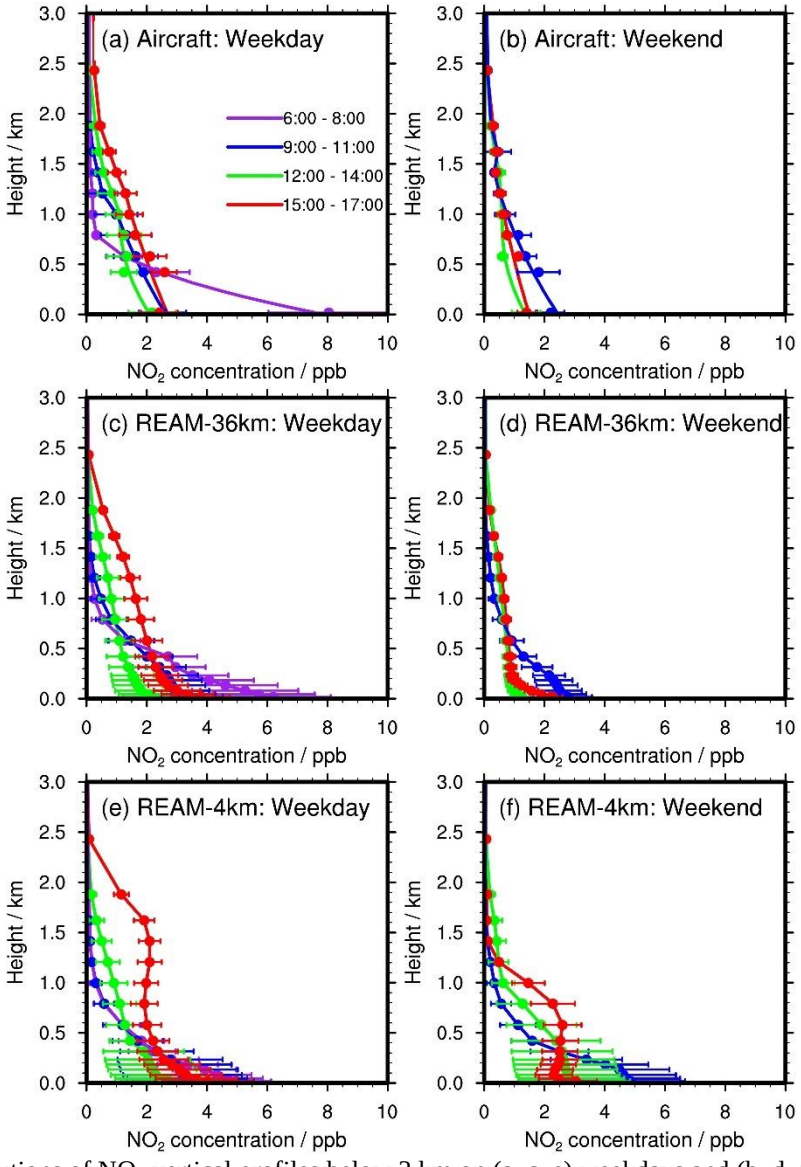

Figure 6. Temporal evolutions of NO_2 vertical profiles below 3 km on (a, c, e) weekdays and (b, d, f) weekends from the (a, b) P-3B aircraft and (c, d) 36-km and (e, f) 4-km REAM during the DISCOVER-AQ campaign. Horizontal bars denote the corresponding standard deviations. In (a) and (b), dots denote aircraft measurements, while lines below 1 km are based on quadratic polynomial fitting, as described in section 2.6. The fitting values are in reasonable agreement with the aircraft and surface measurements in the boundary layer. On weekends, no aircraft observations were made at 6:00 – 8:00 LT, and therefore no corresponding model profiles are shown.

https://doi.org/10.5194/acp-2020-1193
Preprint. Discussion started: 6 January 2021

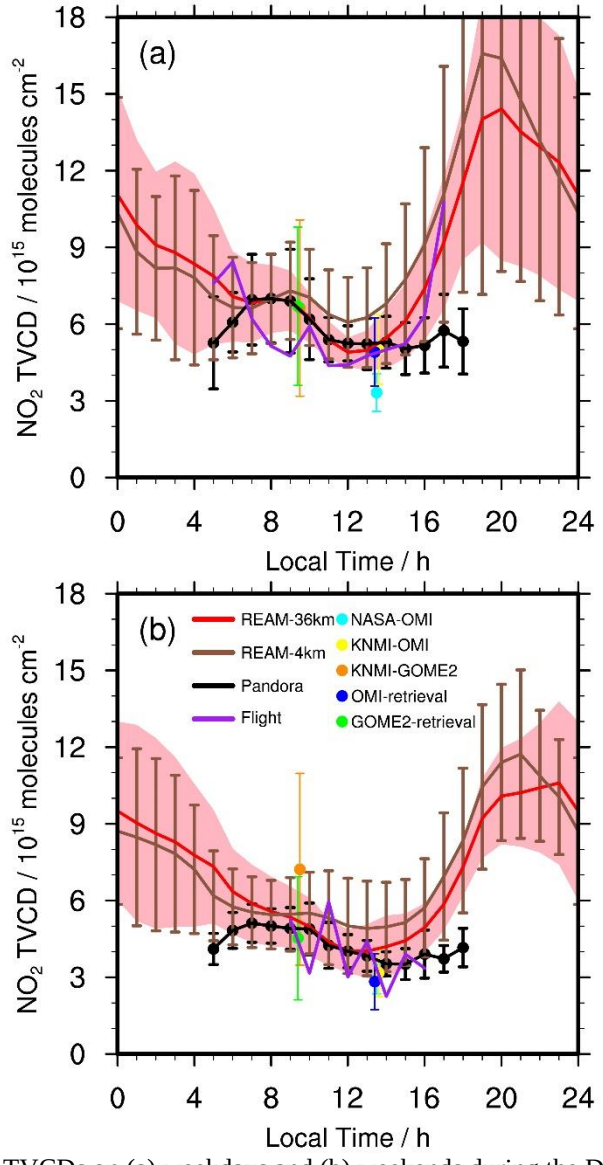

Figure 7. Daily variations of NO_2 TVCDs on (a) weekdays and (b) weekends during the DISCOVER-AQ campaign. "REAM-36km" refers to the 36-km REAM simulation results over the 11 inland Pandora sites. "REAM-4km" refers to the 4-km REAM simulation results over the 11 inland Pandora sites. "Pandora" refers to updated Pandora TVCD data. "Flight" denotes P-3B aircraft-derived NO_2 VCDs below 3.63 km. "NASA-OMI" denotes the OMI NO_2 TVCDs retrieved by NASA over the Pandora sites; "KNMI-OMI" denotes the OMI NO_2 TVCDs from KNMI; "KNMI-GOME2" is the GOME-2A NO_2 TVCDs from KNMI. "OMI-retrieval" and "GOME2-retrieval" denote OMI and GOME-2A TVCDs retrieved by using the KNMI DOMINO algorithm with corresponding 36-km REAM vertical profiles, respectively.

https://doi.org/10.5194/acp-2020-1193
Preprint. Discussion started: 6 January 2021

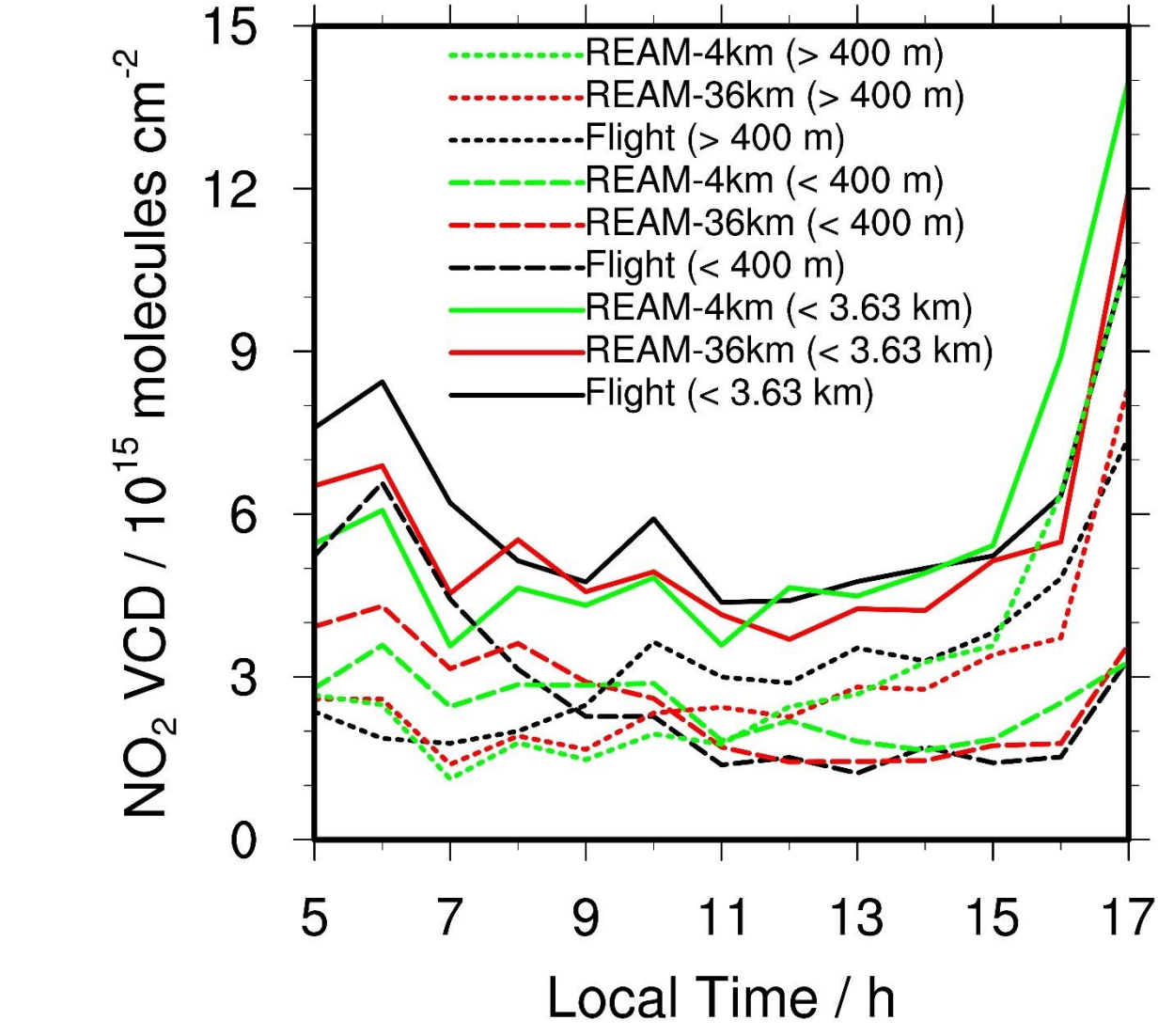

Figure 8. Weekday hourly variations of NO_2 VCDs at different height (AGL) bins (< 3.63 km AGL, < 400 m AGL, and 400 m ~ 3.63 km AGL) based on P-3B aircraft-derived datasets and the 36-km and 4-km REAM results. "Flight" denotes P-3B aircraft-derived NO_2 VCDs, "REAM-36km" denotes coincident 36-km REAM simulated VCDs, and "REAM-4km" denotes coincident 4-km REAM simulated VCDs.

https://doi.org/10.5194/acp-2020-1193
Preprint. Discussion started: 6 January 2021

Atmospheric Chemistry and Physics Discussions

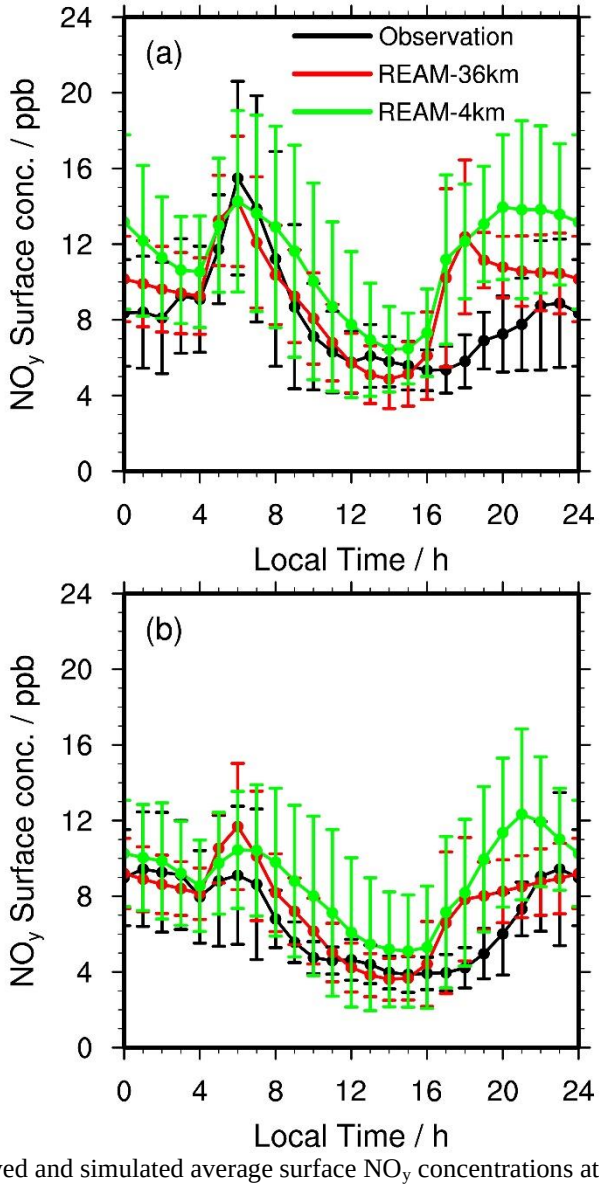

Figure 9. Diurnal cycles of observed and simulated average surface NO_y concentrations at Padonia, Edgewood, Beltsville, and Aldino on (a) weekdays and (b) weekends. Vertical bars denote the corresponding standard deviations. It is noteworthy that the mean NO_x emissions over Padonia, Edgewood, Beltsville, and Aldino are 99% higher in the 4-km than the 36-km REAM simulations (Table S1 and Figure S1).

https://doi.org/10.5194/acp-2020-1193
Preprint. Discussion started: 6 January 2021

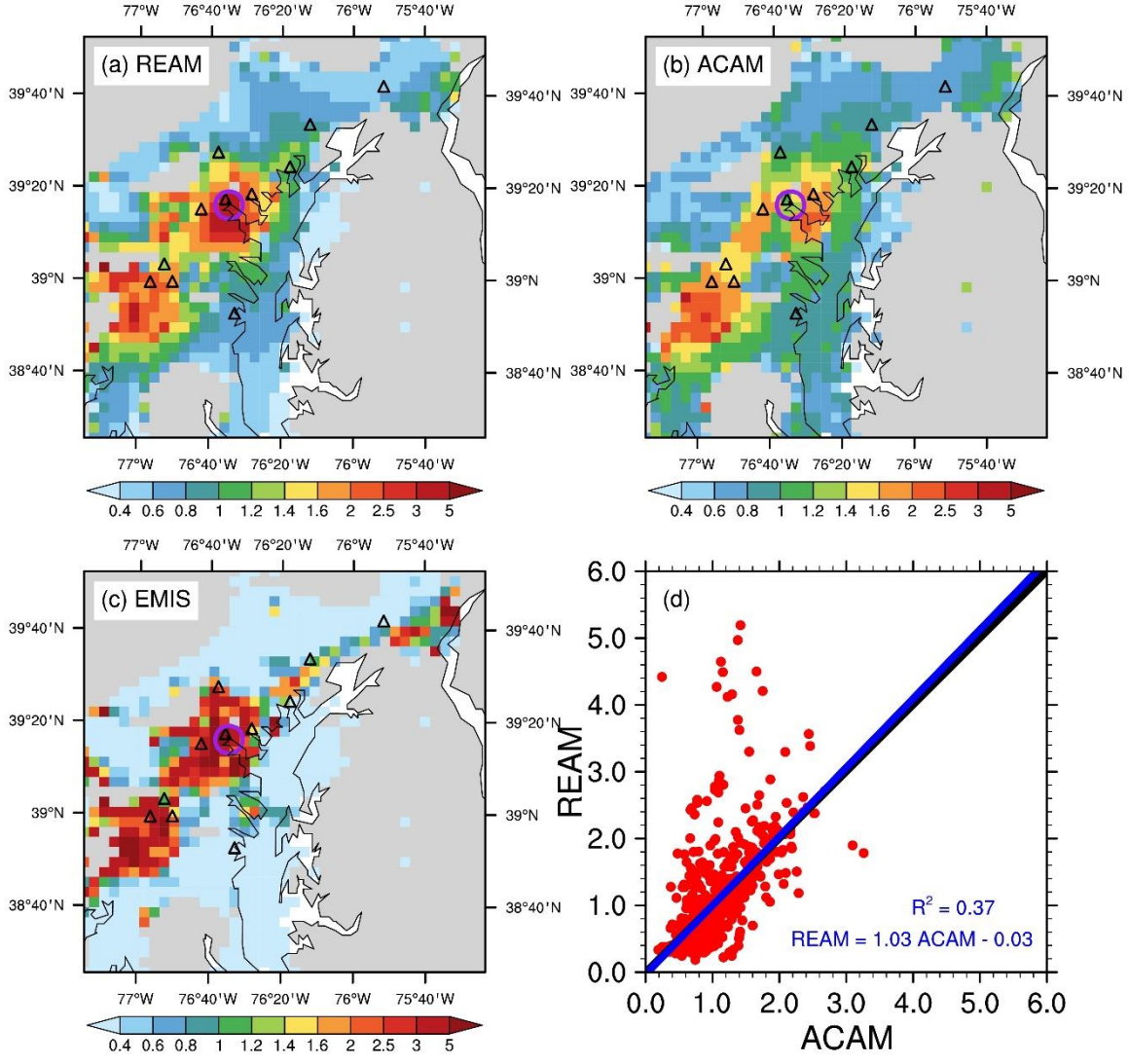

Figure 10. Distributions of the scaled mean (a) ACAM NO_2 VCDs below the UC-12 aircraft and (b) coincident 4-km REAM simulation results on weekdays in July 2011. (c), the distribution of the scaled NEI2011 NO_x emissions on weekdays. (d) is the scatter plot of the scaled ACAM and 4-km REAM NO_2 VCDs from (a) and (b). Here, we scale all values (VCDs and NO_x emissions) based on their corresponding domain averages. The domain averages of ACAM and coincident 4-km REAM NO_2 VCDs are 4.7 ± 2.0 and 4.5 ± 3.2 × 10^{15} molecules cm^{-2}, respectively.